ÉCOLE POLYTECHNIQUE FÉDÉRALE DE LAUSANNE

MATHICSE

Mathematics Institute of Computational Science and Engineering

School of Basic Sciences - Section of Mathematics

MATHICSE Technical Report

Nr. 31.2015

November 2015

Fluid dynamics of an idealized left ventricle: the extended Nitsche's method for the treatment of heart valves as mixed time varying boundary conditions

Anna Tagliabue, Luca Dedè, Alfio Quarteroni

http://mathicse.epfl.ch

Phone: +41 21 69 37648

Address:
EPFL - SB - MATHICSE (Bâtiment MA)
Station 8 - CH-1015 - Lausanne - Switzerland

Fax: +41 21 69 32545

Fluid dynamics of an idealized left ventricle: the extended Nitsche's method for the treatment of heart valves as mixed time varying boundary conditions

Anna Tagliabue [1,*], Luca Dedè [2], and Alfio Quarteroni [1,2,†]

[1] MOX – Modeling and Scientific Computing
Mathematics Department "F. Brioschi"
Politecnico di Milano
via Bonardi 9, Milano, 20133, Italy

[2] CMCS – Chair of Modeling and Scientific Computing
MATHICSE – Mathematics Institute of Computational Science and Engineering
EPFL – École Polytechnique Fédérale de Lausanne
Station 8, Lausanne, CH – 1015, Switzerland

Abstract

In this work, we study the blood flow dynamics in idealized left ventricles (LV) of the human heart modelled by the Navier-Stokes equations with mixed time varying boundary conditions (BCs). The latter are introduced for simulating the functioning of the aortic and mitral valves. Based on the extended Nitsche's method firstly presented in [Juntunen and Stenberg, Mathematics of Computation, 2009], we propose a formulation allowing an efficient and straightforward numerical treatment of the opening and closing phases of the heart valves which are associated to different kind of BCs, namely natural and essential. Moreover, our formulation includes terms preventing the numerical instabilities associated to backflow divergence, i.e. nonphysical reinflow at the valves. We present and discuss numerical results for the LV obtained by means of Isogeometric Analysis for the spatial approximation with the aim of both analysing the formulation and showing the effectiveness of the approach. In particular, we show that the formulation allows to reproduce meaningful results even in idealized LV.

Key words. extended Nitsche's method; mixed time varying boundary conditions; heart fluid dynamics; left ventricle.

[*]Corresponding author. E-mail: anna.tagliabue@polimi.it. Phone: +39 02 2399 4604, Fax: +39 02 2399 4586.
[†]Currently on leave from Politecnico di Milano.

1 Introduction

In the last years, several efforts have been dedicated to describing, studying, and understanding the blood flow dynamics inside the human heart, especially focusing on the human Left Ventricle (LV) [13, 42, 65]. The latter is the heart chamber which distributes the oxygenated blood to the systemic circulation and plays a primal role in the cardiac activity. In particular, due to the recent technological advances in medical imaging techniques [58], a preliminary understanding of the main features characterizing the cardiac hemodynamics has been performed by using e.g. phase-contrast magnetic resonance imaging [41, 38] and by echocardiography techniques [32, 40]. Nevertheless, both of these methods present some deficiencies [13], among which we recall the filtering and reconstruction related to the image processing, the presence of aliasing artefacts, the dependence on the temporal and spatial resolution available, and the use of phase-averaged flows description, which may neglect small-scale instabilities and heart beat to beat variations. More recently, physical and computational models have become of paramount importance in providing more detailed informations on the blood flow features, especially for predicting heart diseases [2, 46, 65]. Indeed, the potentiality of Scientific Computing in understanding the hemodynamics both in physiological and pathological conditions can bring a significant complement to medical imaging or in vitro studies [26], although the complexity of the phenomena at hand remains a challenging task from both the mathematical and numerical points of view. In fact, even if one only focuses on the LV fluid dynamics, the problem should be addressed by accounting for the complex shape of the heart chamber which expands, contracts, and experiences large displacements and, at the same time, whose movement is governed by complex electrical-fluid-structure interactions. Moreover, the blood flow is highly influenced by the presence of the valves that yield an additional fluid-structure interaction problem, with a regime varying during the heart beat from laminar to transitional, and eventually turbulent [13]. Because of these aspects and the additional difficulty in obtaining accurate clinical data describing, e.g., the mechanical properties of the wall or the blood flow profile through the mitral valve, simplified models have been introduced and studied, starting from the earliest works based on the immersed boundary method [51, 52, 53, 47] up to more recent studies, e.g. [1, 2, 20, 21, 22, 67].

In this work, we perform a preliminary study of the hemodynamics inside the LV by considering an idealized LV represented as a truncate prolate ellipsoid, whose motion is prescribed by a wall law. By assuming a Newtonian rheology for the blood flow, we model it by the incompressible Navier-Stokes equations in the Arbitrary Lagrangian Eulerian (ALE) formulation [23, 24, 25, 27, 28], which we spatially approximate by using Isogeometric Analysis (IGA) [3, 5, 16]. Indeed, in the last years, IGA has been largely used for the numerical approximation of a wide range of problems providing accurate and efficient solutions, also in the context of cardiovascular system modelling [5, 62]. Specifically, we refer to NURBS-based IGA [16] in the framework of the Galerkin method, both for the mathematical properties of the basis functions, e.g. NURBS basis functions which can be globally $\mathcal{C}^k$-continuous in the computational domain for some $0 \leq k \leq p-1$, with p the polynomial degree, and for the possibility to exactly represent conic sections, as it is the idealized LV. Indeed, the configuration of a truncate prolate spheroid used as idealized LV is considered in literature [1, 2] as a sufficiently accurate geometry to represent the average endocardial shape of different human subjects; in our model, the motion of the LV is completely defined through time variations of the upper diameter and of the major semi-axis of the ellipsoid. Such time dependent functions should, in principle, be computed by solving an electrical-fluid-structure interaction problem; however, in the present work we instead prescribe the ventricle wall displacement derived from a simple elastic

model and a flow-discharge function following [1, 2].

In describing the complex fluid dynamics in the LV, which includes asymmetric vortex structures allowing an efficient filling and a natural redirection towards the aorta, one of the most difficult aspects consists in accounting for the valves in a realistic and physiologically meaningful manner. In this respect, this work focuses on the formulation of mixed time varying (MTV) boundary conditions (BCs) for the Navier-Stokes equations which allow a simplified but realistic treatment of the mitral and aortic valves for the study of the LV fluid dynamics. Specifically, we propose a weak treatment of such BCs by embedding the valves opening and closing phases into the variational formulation of the problem. Indeed, we remark that, from both the mathematical and numerical points of view, accounting for the presence of the valves through commonly used BCs is a challenging task due to the different nature of the BCs associated to the opening and closing phases, which namely switch during the heart beat from essential to natural and viceversa. In this respect, even the well-posedness analysis of a simpler equation, as a parabolic equation, requires a careful treatment [57].

The formulation of these new kind of MTV BCs for the Navier-Stokes equations in ALE formulation is done in the framework of the extended Nitsche's method (ENM) firstly proposed by Juntunen and Stenberg [36]. Specifically, by using a penalty technique we allow the switching in time between the imposition of Dirichlet and defective BCs of natural type [5, 31, 63]. On the one hand, the Dirichlet BCs are imposed weakly rather than strongly in the test functions space and it has been shown in [7, 8, 33] that this leads to a better resolution of boundary layers with respect to the strong imposition, eventually avoiding computationally expensive fine meshes. On the other hand, when imposing defective BCs of the natural type, we consider additional terms with respect to the standard imposition of the natural BCs in weakly formulated problems; these additional terms control the backflow velocity through the outflow. In particular, such terms prevent the numerical instabilities associated to backflow divergence [49] without neither perturbing physically the problem nor introducing additional unknowns, as e.g. for the Lagrange multiplier method [39]; in addition, the consistency of the method is also preserved. Controlling backflow divergence is very important for the LV; indeed, the LV fluid dynamics is potentially affected by such behaviour correspondingly to the outlet LV boundary representing the open aortic valve, possibly leading to numerical instabilities due to partial or total flow reversal, as well as local flow recirculation.

Because of the similar behaviour of the mitral and aortic valves, both of which undergo opening and closing processes, we use the MTV BCs for both of the valves modelled as orifices of infinitesimal thickness located at the upper equatorial diameter of the idealized LV. Nevertheless, we further improve the formulation of the BCs on the mitral valve by adding a regularizing high order boundary term in a penalty fashion which induces somehow realistic inlet profiles. Indeed, although there is a general lack of accurate clinical data describing the inflow profile through the mitral valve, it has been highlighted from visualizations [9, 55] that the mitral valve has a strong influence on the intra-ventricular vortex structures. As a matter of fact, the study of the fluid dynamics of the LV, even in an idealized setting, cannot neglect an accurate and physically meaningful modelling of the aortic and mitral valves. Therefore, in this paper, we propose a general framework for modelling the valves functioning by means of mixed type BCs of the Navier-Stokes equations that are treated numerically by means of the ENM.

The outline of this work is as follows. In Sec. 2, we define the problem of modelling the blood flow in an idealized two-dimensional LV for which we consider the incompressible Navier-Stokes equations in ALE formulation; we describe the LV geometry and the governing law for the imposed LV motion. In Sec. 3 we recall the Galerkin method in the framework of NURBS-based IGA with

VMS-LES formulation [4, 12, 62] and the generalized-α method [14, 35, 66] for the discretization in space and time, respectively. In Sec. 4, we provide the formulation of the MTV BCs for the Navier-Stokes equations describing the valves; the equations are approximated by using the ENM. Firstly, we focus on modelling the aortic valve, then we extend it to the mitral valve by introducing a suitable regularizing term yielding realistic inflow velocity profiles. Finally, in Sec. 5, we present and discuss some numerical results regarding the fluid dynamics of the LV and show the effectiveness of the method compared to results available in literature. Conclusions follow.

2 Modeling of blood flows in the idealized left ventricle

We describe the model for the blood flow in an idealized LV. In Sec. 2.1, by assuming a Newtonian rheology for the fluid in an expanding and contracting cavity undergoing large displacements, we consider the incompressible Navier-Stokes equations in ALE formulation [5, 23, 24, 25, 27, 28]. In Sec. 2.2, we describe a two-dimensional idealized LV geometry, in first approximation half of an ellipse [1, 64, 67]. We focus on a model with prescribed wall movement, for which the governing law associated to the mechanical LV displacement following [1, 2]. Finally, in Sec. 2.4, we describe the mathematical formulation of a set of BCs able to describe a physiologically compatible two-dimensional LV model.

2.1 Navier-Stokes equations in ALE formulation

Let $\Omega^{(t)} \subset \mathbb{R}^d$, with $d = 2$ or 3, be a time dependent spatial domain with boundary $\partial\Omega^{(t)}$ representing the configuration at the current time $t \in (0,T)$ of a reference domain $\widehat{\Omega} \subset \mathbb{R}^d$. Specifically, the reference domain is mapped to the current configuration through the ALE mapping $\phi^{(t)} : \widehat{\Omega} \to \Omega^{(t)}$; we indicate with $\mathbf{x}$ and $\mathbf{X}$ the spatial coordinates of the current and reference configurations, respectively. The dimensionless Navier-Stokes equations for an incompressible fluid in ALE (convective) formulation read:

for all $t \in (0,T)$, find $\boldsymbol{u} : \Omega^{(t)} \to \mathbb{R}^d$ and $p : \Omega^{(t)} \to \mathbb{R}$ such that:

$$\begin{cases} \left.\dfrac{\partial \boldsymbol{u}}{\partial t}\right|_{\mathbf{X}} + ((\boldsymbol{u} - \widehat{\boldsymbol{u}}) \cdot \nabla)\, \boldsymbol{u} - \nabla \cdot \sigma(\boldsymbol{u}, p) = \boldsymbol{f} & \text{in } \Omega^{(t)}, \quad (2.1a) \\ \nabla \cdot \boldsymbol{u} = 0 & \text{in } \Omega^{(t)}, \quad (2.1b) \end{cases}$$

complemented with suitable initial and boundary conditions, where the partial time derivative is taken with respect to the (fixed) reference domain $\widehat{\Omega}$, while the partial spatial derivatives are evaluated in the current configuration. The vector field $\boldsymbol{f} : \Omega^{(t)} \to \mathbb{R}^d$ for all $t \in (0,T)$ indicates the *external body forces* and $\widehat{\boldsymbol{u}}$ is the (unknown) domain velocity. Moreover, the Cauchy stress tensor $\sigma(\boldsymbol{u}, p)$ is defined as $\sigma(\boldsymbol{u}, p) = -p\mathrm{I} + \dfrac{2}{\mathbb{R}e} D(\boldsymbol{u})$, with $\mathbb{R}e$ the Reynolds number, $D(\boldsymbol{u}) := \dfrac{(\nabla \boldsymbol{u} + \nabla \boldsymbol{u}^T)}{2}$ is the strain rate tensor, and I is the identity tensor. The initial condition of the fluid velocity is a divergence-free velocity field $\boldsymbol{u}_0 : \Omega^{(0)} \to \mathbb{R}^d$. Moreover, we consider either essential or natural BCs [5, 6], the latter associated to the total momentum flux:

$$\boldsymbol{\Phi}(\boldsymbol{u} - \widehat{\boldsymbol{u}}; \boldsymbol{u}, p) = -\boldsymbol{u} \otimes (\boldsymbol{u} - \widehat{\boldsymbol{u}}) + \sigma(\boldsymbol{u}, p), \quad (2.2)$$

as we will detail in Sec. 2.4. Specifically, if the Dirichlet and natural BCs are expressed in terms of the vector fields $\boldsymbol{g}$ and $\boldsymbol{G}$, these read for any $t \in (0,T)$:

$$\boldsymbol{u} = \boldsymbol{g} \quad \text{on } \Gamma_D^{(t)}, \tag{2.3a}$$

$$-\boldsymbol{\Phi}(\boldsymbol{u} - \widehat{\boldsymbol{u}}; \boldsymbol{u}, p)\mathbf{n} = \boldsymbol{G} \quad \text{on } \Gamma_N^{(t)}, \tag{2.3b}$$

respectively, where $\Gamma_D^{(t)}$ and $\Gamma_N^{(t)}$ are subsets of $\partial\Omega^{(t)}$ at any time $t \in (0,T)$ and $\mathbf{n}$ indicates the outward directed unit vector normal to $\Gamma_N^{(t)}$.

The weak formulation of Eq. (2.1) complemented with the BCs (2.3) considers the following time dependent trial and weighting spaces for the velocity field at $t \in (0,T)$:

$$\mathcal{V}_{\boldsymbol{g}}^{(t)} := \{\boldsymbol{u} \in [\mathrm{H}^1(\Omega^{(t)})]^d : \boldsymbol{u} = \boldsymbol{g} \quad \text{on } \Gamma_D^{(t)}\}, \tag{2.4a}$$

$$\mathcal{W}^{(t)} \equiv \mathcal{V}_{\boldsymbol{0}}^{(t)} := \{\boldsymbol{u} \in [\mathrm{H}^1(\Omega^{(t)})]^d : \ \boldsymbol{u} = \boldsymbol{0} \quad \text{on } \Gamma_D^{(t)}\}, \tag{2.4b}$$

respectively, while for the pressure we use $\mathcal{Q}^{(t)} := \mathrm{L}^2(\Omega^{(t)})$. Then, the variational formulation of problem (2.1) reads:

$$\text{for all } t \in (0,T), \text{ find } (\boldsymbol{u},p) \in \mathcal{V}_{\boldsymbol{g}}^{(t)} \times \mathcal{Q}^{(t)} : \quad \mathcal{B}((\boldsymbol{\varphi},q),(\boldsymbol{u},p);\widehat{\boldsymbol{u}}) = \mathcal{F}(\boldsymbol{\varphi},q) \quad \forall (\boldsymbol{\varphi},q) \in \mathcal{W}^{(t)} \times \mathcal{Q}^{(t)}, \tag{2.5}$$

where:

$$\begin{aligned}\mathcal{B}((\boldsymbol{\varphi},q),(\boldsymbol{u},p);\widehat{\boldsymbol{u}}) := &\int_{\Omega^{(t)}} \boldsymbol{\varphi} \cdot \frac{\partial \boldsymbol{u}}{\partial t}\, \mathrm{d}\Omega + \frac{2}{\mathbb{R}e}\int_{\Omega^{(t)}} D(\boldsymbol{\varphi}) : D(\boldsymbol{u})\, \mathrm{d}\Omega + \int_{\Omega^{(t)}} \boldsymbol{\varphi} \cdot ((\boldsymbol{u} - \widehat{\boldsymbol{u}}) \cdot \nabla)\, \boldsymbol{u}\, \mathrm{d}\Omega \\ &- \int_{\Omega^{(t)}} p\, \nabla \cdot \boldsymbol{\varphi}\, \mathrm{d}\Omega + \int_{\Omega^{(t)}} q\, \nabla \cdot \boldsymbol{u}\, \mathrm{d}\Omega,\end{aligned} \tag{2.6a}$$

$$\mathcal{F}(\boldsymbol{\varphi},q) := \int_{\Omega^{(t)}} \boldsymbol{\varphi} \cdot \boldsymbol{f}\, \mathrm{d}\Omega + \int_{\Gamma_N^{(t)}} \boldsymbol{\varphi} \cdot \boldsymbol{G}\, \mathrm{d}\Gamma. \tag{2.6b}$$

2.2 Left ventricle geometry and wall displacements

We consider now the two-dimensional case, for which $d = 2$. We geometrically represent the LV as half of an ellipse with moving walls characterized by the time dependent functions $D : (0,T) \to \mathbb{R}$ and $H : (0,T) \to \mathbb{R}$ representing the upper diameter and the major semiaxis of the ellipsoid, respectively; see Fig. 1a. The geometry at the beginning of the diastolic filling phase is taken as the reference configuration $\widehat{\Omega}$; the diameter of the reference configuration is $D(0) \equiv D_0 = 3.4$ cm with x coordinate between -1.7 cm and 1.7 cm, moreover D_0 is chosen as the reference lengthscale (L_0). Similarly, we set the height $H(0) = H_0 = 6.8$ cm, for which $H_0/D_0 = 2$ as e.g. in [21]; the base of the ellipsoid is fixed, for which the apex is moving during the heart beat.

The inlet and outlet subsets of the boundary representing the mitral and aortic valves are located on the upper part of the LV. In the reference configuration, the mitral valve position is fixed between the x coordinates -0.085 cm and 1.615 cm, while the aortic valve is fixed between the x coordinates -1.632 cm and -0.272 cm. Their positions and sizes are fixed in time, despite the LV base moves accordingly with the governing wall movement law, described in Sec. 2.3.

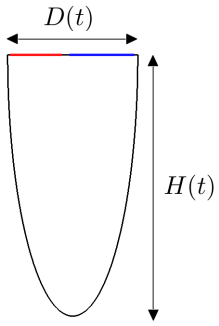

(a) Idealized 2D LV geometry.

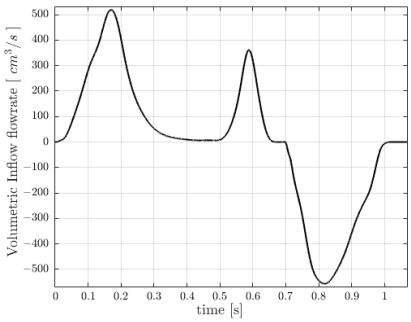

(b) Volumetric flow rate $Q_V(t)$ vs. time t for a 3D LV.

Figure 1: Geometry representing the idealized human LV (1a) with the aortic valve in red and mitral valve in blue; flow rates in a 3D LV (1b).

2.3 Prescribed wall displacement of the left ventricle

The large displacements experienced by the LV wall and the strong fluid-structure interactions (FSI) play a fundamental rule in the LV flow. In the present work, we do not analyse the FSI problem governed by the coupling of the fluid and wall dynamics; rather we refer the interested reader to e.g. [43] for a state of the art in FSI problem for the LV. In this paper, we are more interested in the fluid dynamics aspects by prescribing a priori the LV wall displacement based on a simple elastic model and a given flow-discharge profile, following [1, 2]. We remark that for patient-specific LV geometries, a time dependent ventricle model derived from in vivo images data (MRI, Echocardiography) could be used; see e.g. [37, 46].

We prescribe the LV wall motion as a dilatation map by controlling the time evolution of the equatorial diameter $D(t)$ and the LV height $H(t)$. We recall that, in literature [13, 21, 45, 67], for the idealized human LV the ratio between H and D is typically fixed at $H(0)/D(0) \simeq 1.7 \div 2$. During the cardiac cycle, this ratio basically varies in this range, as shown in Fig. 2b and it is determined by the governing law used to prescribe the LV wall movement.

Following [1], we consider $D(t)$ and $H(t)$ for a three-dimensional LV as the solution of the system of ordinary differential equations:

$$\text{find } D:(0,T)\to\mathbb{R} \text{ and } H:(0,T)\to\mathbb{R}: \quad \begin{cases} \dfrac{\mathrm{d}D}{\mathrm{d}t} = \dfrac{6Q}{\pi}\dfrac{8H^2-D^2}{20DH^3-2HD^3} & \text{in } (0,T), \quad (2.7a) \\ \dfrac{\mathrm{d}H}{\mathrm{d}t} = \dfrac{H}{D}\dfrac{\mathrm{d}D}{\mathrm{d}t}\dfrac{4H^2}{8H^2-D^2} & \text{in } (0,T), \quad (2.7b) \\ D(0) = D_0, & (2.7c) \\ H(0) = H_0. & (2.7d) \end{cases}$$

The system (2.7) has been derived in [1] by considering a simplified elastic membrane model and enforcing the equality of the volumetric flow rate and LV volume variation, i.e. $Q_V(t) := \dfrac{\mathrm{d}V}{\mathrm{d}t}(t)$ for all $t \in (0,T)$, where the three-dimensional LV volume is $V(t) = \dfrac{\pi}{6}D^2(t)H(t)$. The prescribed inlet/outlet volumetric discharge Q_V, reported in Fig. 1b and used in [2], has been adapted from clinical data and it is characterized by two maxima, the first corresponding to the early LV filling (E-wave) and the secondary filling mainly associated to the atrial contraction (A-wave). Negative values of Q_V, instead, represent the systolic phase in which the ventricle contracts. Once $H(t)$

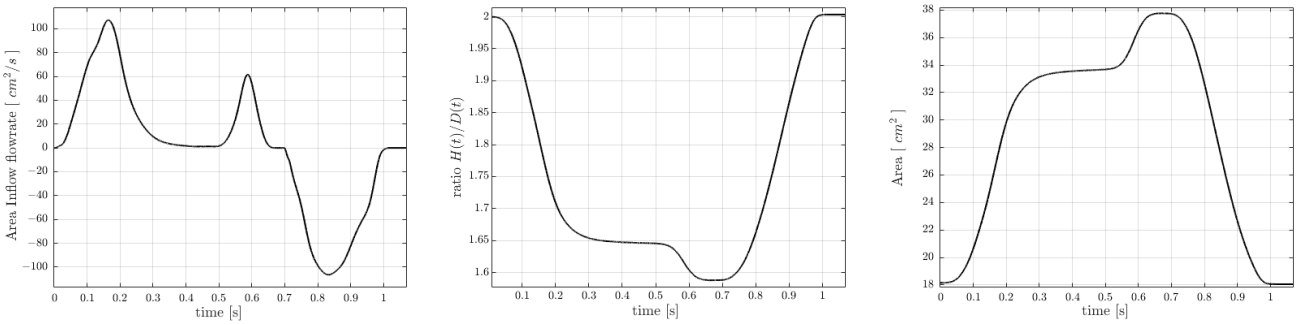

(a) Area flow rate $Q(t)$ vs. time t for a 2D LV.

(b) Ratio between the height ($H(t)$) and the upper diameter ($D(t)$) vs. time.

(c) Area $A(t)$ vs. time t for a 2D LV.

Figure 2: Flow rates for a 2D LV (2a); evolution of the ratio $H(t)/D(t)$ vs. time [s] for one heart beat (2b) and evolution of the area $A(t)$ for 2D LV vs. time [s] in an heart beat (2c).

and $D(t)$ are obtained by solving problem (2.7), for example by means of the explicit Runge-Kutta method [11], we deduce, for the two-dimensional LV model, both the area and the *area flow rate*, defined as the time variation of the area and whose profile is reported in Figure 2a. Specifically, these are given by $A(t) := \frac{\pi}{4} D(t)H(t)$ and $Q(t) = \frac{\mathrm{d}A}{\mathrm{d}t}(t) = \frac{\pi}{4} D(t)H(t) \left(\frac{1}{D(t)} \frac{\mathrm{d}D}{\mathrm{d}t}(t) + \frac{1}{H(t)} \frac{\mathrm{d}H}{\mathrm{d}t}(t) \right)$, for all $t \in (0, T]$, respectively. In Fig. 2c, we report the area variation of the LV vs. the time for an heart beat, i.e. $A(t)$ vs t. Moreover, we obtain the functions $\lambda : (0, T) \to \mathbb{R}$ and $\mu : (0, T) \to \mathbb{R}$ given by $\lambda(t) := \frac{D(t)}{D_0}$ and $\mu(t) := \frac{H(t)}{H_0}$, respectively, which define the affine transformation governing the LV chamber dilatation and whose derivatives provide the velocity at the boundary, as $\boldsymbol{v}^{\mathrm{W}}(\mathbf{x}, t) := \left(\frac{\mathrm{d}}{\mathrm{d}t} \lambda(t) \cdot \mathrm{x}, \frac{\mathrm{d}}{\mathrm{d}t} \mu(t) \cdot \mathrm{y} \right)$.

2.4 Boundary conditions for physiological flows in the left ventricle

We are interested in properly accounting for the valves effects in the idealized LV by prescribing suitable, physiologically compatible BCs. In this respect, on the subset of the boundary $\partial\Omega^{(\mathrm{t})}$ corresponding to the muscle LV walls, say $\Gamma^{\mathrm{W},(t)}$ for any $t \in (0, T)$, we impose the so called *no-slip condition*, a Dirichlet BC, which reads for any $t \in (0, T)$:

$$\boldsymbol{u} = \boldsymbol{v}^{\mathrm{W}} \quad \text{on } \Gamma^{\mathrm{W},(\mathrm{t})}, \tag{2.8}$$

where $\boldsymbol{v}^{\mathrm{W}}$ denotes the velocity of the LV wall, determined by the expressions of $\frac{\mathrm{d}D}{\mathrm{d}t}$ and $\frac{\mathrm{d}H}{\mathrm{d}t}$ in Eq. (2.7). The remaining part of the boundary is constituted by the subsets Γ^{AO} and Γ^{MT} which correspond to the aortic and mitral valves, respectively, modelled as orifices of infinitesimal thickness; in terms of Eq. (2.3), $\Gamma^{\mathrm{W},(\mathrm{t})} \subseteq \Gamma_D^{(\mathrm{t})}$ and $\boldsymbol{g} = \boldsymbol{v}^{\mathrm{W}}$ on $\Gamma^{\mathrm{W},(\mathrm{t})}$.

A common practice [1, 2, 20, 21, 22, 46], motivated by physical considerations, consists in prescribing a velocity profile on Γ^{MT}, i.e. a Dirichlet condition on Γ^{MT}. In the first instance, we follow this approach focusing on the aortic valve to account through suitable BCs the opening and closing stages; the latter are associated to different types of BCs, namely, essential and natural, which switch during the heart beat. A similar treatment can be applied to the mitral valve.

2.4.1 Prescribed inflow velocity at the mitral valve: pulsatile flow

The filling of the LV chamber occurs through the mitral valve in two steps, the Early-filling wave (E-wave) and the A-wave. In physiological conditions, the blood enters the LV as an impulsive jet which is redirected toward one portion of the moving wall and interacts with it, due to the asymmetric position of the mitral valve with respect to the central axis of the LV. There is a strong dependence of the intraventricular fluid dynamics on the inflow velocity [1], and specifically, on the intensity of the E- and A- filling waves, the velocity profile, and the size and shape of the mitral valve orifice.

First, we consider a prescribed pulsatile periodic flow with either parabolic or flat velocity profiles compatible with the flow rate $Q(t)$ of Fig. 2a. In this respect, by denoting with ϵ_{MT} the eccentric position of the mitral orifice with respect to the vertical axis of the LV and with r_{MT} the radius of the mitral orifice, respectively, we assume that the function $\boldsymbol{g}^{\text{MT}}$ defining the Dirichlet BC of Eq. (2.3a) on Γ^{MT} reads:

$$\boldsymbol{g}^{\text{MT}} : \Gamma^{\text{MT}} \times (0,T) \to \mathbb{R}^2 \quad : \quad \boldsymbol{g}^{\text{MT}}(\mathbf{x},t) := \boldsymbol{v}^{\text{MT}}(\mathbf{x}) q(t), \tag{2.9}$$

with $\boldsymbol{v}^{\text{MT}} : \Gamma^{\text{MT}} \to \mathbb{R}^2$ and $q : (0,T) \to \mathbb{R}$ a vector and a scalar valued functions, respectively. Specifically, by considering dimensionless quantities for Q, ϵ_{MT} and r_{MT}, we define $q(t) := Q(t)\chi_{\{Q(t)>0\}}$ and $\boldsymbol{v}^{\text{MT}} := \left(\boldsymbol{v}_{\text{x}}^{\text{W}}, \frac{1}{c_{\text{NI}}} exp\left\{-\left(\frac{\text{x}-\epsilon_{\text{MT}}}{r_{\text{MT}}}\right)^8\right\}\right)$ or $\boldsymbol{v}^{\text{MT}} := \left(\boldsymbol{v}_{\text{x}}^{\text{W}}, \frac{6}{8}(\text{x}^2 - 2\epsilon_{\text{MT}}\text{x} + {\epsilon_{\text{MT}}}^2 - {r_{\text{MT}}}^2)\right)$ for flat or parabolic velocity inlet profiles, respectively; c_{NI} is such that $\int_{-r_{\text{MT}}}^{r_{\text{MT}}} \frac{1}{c_{\text{NI}}} exp\left\{-\left(\frac{\text{x}-\epsilon_{\text{MT}}}{r_{\text{MT}}}\right)^8\right\} = 1$ in analogy with [20].

2.4.2 Boundary conditions for the treatment of the aortic valve

For the modeling of the aortic valve, we consider essential BCs as no-slip BCs when the valve is closed, while natural BCs when open. In particular, for this latter stage, in order to ensure realistic simulations and to account for the downstream circulation in the aorta, a geometrical multiscale approach can be reproduced in a simplified manner by considering resistance or defective BCs at Γ^{AO} [5, 6, 63]. Specifically, we prescribe at the open aortic valve orifice a resistance BCs of the natural type, similarly to [5, 6]. In this case, on $\Gamma_N^{(t)} := \begin{cases} \emptyset & \text{if } Q(t) \geq 0, \\ \Gamma^{\text{AO}} & \text{if } Q(t) < 0, \end{cases}$ we consider the BC given in Eq. (2.3b) by decomposing the prescribed stress on $\Gamma_N^{(t)}$ in its normal and tangential components as $\boldsymbol{G} := G_\perp \mathbf{n} + G_\parallel \mathbf{t}$, with $\mathbf{t}$ the unit tangent vector to $\Gamma_N^{(t)}$. Specifically, we set $G_\parallel = 0$ and $G_\perp = -(C_{\text{out}} Q_{\text{out}}^{\text{AO}} + P_V)$. The coefficient C_{out} represents a *resistance constant*, whose corresponding dimensional counterpart has dimensions in the units dyn·s/cm^5 and whose values can be obtained by *in vivo* measurements [56]. The term P_V sets a physiologically realistic pressure. Finally, $Q_{\text{out}}^{\text{AO}}$ refers to the flowrate through Γ^{AO}, which we indicate as $Q_{\text{out}}^{\text{AO}} := \frac{\pi}{2} r_{AO} \int_{\Gamma^{\text{AO}}} \boldsymbol{u} \cdot \mathbf{n} \, \mathrm{d}\Gamma$, with r_{AO} the radius of the aortic orifice.

We remark that numerical instabilities may arise with natural BCs on Γ^{AO} in the presence of back flow reversal [49]; to overcome this drawback in [6] the defective BC is augmented by a term acting only in presence of reversal flow. Instead, we refer to the form proposed in [5] which does

not add any add hoc term to control back flow reversal, and allows a straightforward treatment in the framework of the ENM.

3 Numerical approximation of the Navier-Stokes equations

To numerically approximate the incompressible Navier-Stokes equations in ALE formulation (2.5), we consider IGA in the framework of the Galerkin method [3, 5, 16, 18] for its spatial approximation, while the time discretization with the generalized-α method [14, 35, 66]. Specifically, in order to provide a stable formulation in the sense of the inf-sup condition [10, 54], to control the numerical instabilities due to the advective regime occurring at high Reynolds numbers, and to numerically model turbulence under the Large Eddy Simulation paradigm, we consider the Variational Multiscale Method with terms accounting for LES modeling (VMS-LES) [4]. In Sec. 3.2, we provide the semi-discrete formulation in space based on the Galerkin method in the framework of NURBS-based IGA with VMS-LES formulation, that we later fully discretize by the generalized-α method.

3.1 Spatial approximation: IGA

In order to semi-discretize the problem (2.5) for any $t \in (0,T)$, we firstly represent the reference domain $\widehat{\Omega}$ as a NURBS geometry and we observe that the idealized two-dimensional LV can be exactly represented by quadratic NURBS; see e.g. [16, 17, 18]. We remark that, with the Finite Element method only an approximation of Ω with a polygonal shaped domain Ω_h can be obtained; this induces a geometrical error which potentially perturbs the formulation of the ENM.

Let $\{\widehat{\mathbf{P}}_A\}_{A=1}^{N_b}$ and $\{\widehat{\boldsymbol{N}}_A\}_{A=1}^{N_b}$ be the control points and the set of NURBS basis functions defining the NURBS geometry as $\mathbf{X} = \sum_{A=1}^{N_b} \widehat{\mathbf{P}}_A \widehat{\boldsymbol{N}}_A(\mathbf{X})$. Then, the discrete ALE mapping is defined as:

$$\phi^{(t)}(X) := \sum_{A=1}^{N_b} (\widehat{\mathbf{P}}_A + \mathbf{d}_A(t)) \widehat{\boldsymbol{N}}_A(\mathbf{X}) \tag{3.1}$$

where $\{\mathbf{d}_A(t)\}_{A=1}^{N_b}$ are the displacement vectors of the control points associated to the prescribed displacement of the LV. As consequence, we obtain a representation of the current configuration $\Omega^{(t)}$, whose NURBS mesh is denoted by $\mathcal{T}_h^{(t)}$, with $h_T^{(t)} := \operatorname{diam} T^{(t)}$ the diameter of a general element $T^{(t)} \in \mathcal{T}_h^{(t)}$ and $h^{(t)} := \max_{T^{(t)} \in \mathcal{T}_h^{(t)}} h_T^{(t)}$ the characteristic mesh size. Moreover, we define the space of NURBS in $\Omega^{(t)}$ as the push-forward of the space $\widehat{\mathcal{N}}_h := \operatorname{span}\{\widehat{\boldsymbol{N}}_A\}_{A=1}^{N_b}$, i.e. $\mathcal{N}_h^{(t)} := \operatorname{span}\{\widehat{\boldsymbol{N}}_A \circ {\phi^{(t)}}^{-1}\}_{A=1}^{N_b} = \operatorname{span}\{\boldsymbol{N}_A^{(t)}\}_{A=1}^{N_b}$.

The problem (2.5) is formulated in terms of $(\boldsymbol{u}, p)$ in the current configuration. When considering NURBS-based IGA in the framework of the Galerkin method, we look for an approximate solution as an element of the NURBS space $\mathcal{N}_h^{(t)}$, i.e. $\boldsymbol{u}_h(\mathbf{x},t) := \sum_{A=1}^{N_b} \boldsymbol{u}_A(t) \boldsymbol{N}_A^{(t)}(\mathbf{x})$ and $p_h(\mathbf{x},t) := \sum_{A=1}^{N_b} p_A(t) \boldsymbol{N}_A^{(t)}(\mathbf{x})$, where $\{\boldsymbol{u}_A(t)\}_{A=1}^{N_b}$ and $\{p_A(t)\}_{A=1}^{N_b}$ are the control variables

associated to the velocity and the pressure at $t \in (0,T)$, respectively. Specifically, the semi-discrete formulation of problem (2.5), reads:

for all $t \in (0,T)$, find $(\boldsymbol{u}_h, p_h) \in \mathcal{V}_h^{(t)} \times \mathcal{Q}_h^{(t)}$:

$$\mathcal{B}((\boldsymbol{\varphi}_h, q_h), (\boldsymbol{u}_h, p_h); \widehat{\boldsymbol{u}}_h) = \mathcal{F}(\boldsymbol{\varphi}_h, q_h), \quad \forall (\boldsymbol{\varphi}_h, q_h) \in \mathcal{W}_h^{(t)} \times \mathcal{Q}_h^{(t)}, \tag{3.2}$$

where $\mathcal{V}_h^{(t)} := \mathcal{V}^{(t)} \cap \mathcal{N}_h^{(t)}$, $\mathcal{W}_h^{(t)} := \mathcal{W}^{(t)} \cap \mathcal{N}_h^{(t)}$, and $\mathcal{Q}_h^{(t)} := \mathcal{Q}^{(t)} \cap \mathcal{N}_h^{(t)}$; the form $\mathcal{B}((\boldsymbol{\varphi}_h, q_h), (\boldsymbol{u}_h, p_h); \widehat{\boldsymbol{u}}_h)$ and the functional $\mathcal{F}(\boldsymbol{\varphi}_h, q_h)$ read as in Eqs. (2.6a) and (2.6b), respectively.

3.2 VMS-LES modeling of the Navier-Stokes equations in ALE formulation

Due to the fact that we are considering a couple of spaces which does not satisfy the Babuška-Brezzi condition [10, 54] as the same basis functions are used for both the velocity and the pressure spaces, we need to consider a stabilized Galerkin formulation of the Navier-Stokes equations. Although several stabilized methods can be used to overcome this issue, see e.g. [10], we consider the Variational Multiscale formulation for Large Eddy simulation (VMS-LES) [4]. The method yields a stable formulation in the sense of inf-sup problem, controls numerical instabilities due to transport dominated regime, and provide LES modeling of turbulence. The latter method has been firstly proposed in [4], then further developed in [16, 17, 18] and extended to the ALE case in [5, 62]. Problem (3.2) in VMS-LES formulation reads:

for all $t \in (0,T)$, find $(\boldsymbol{u}_h, p_h) \in \mathcal{V}_h^{(t)} \times \mathcal{Q}_h^{(t)}$:

$$\mathcal{R}^{\text{VMS}}((\boldsymbol{\varphi}_h, q_h), (\boldsymbol{u}_h, p_h); \widehat{\boldsymbol{u}}_h) = 0 \quad \forall (\boldsymbol{\varphi}_h, q_h) \in \mathcal{W}_h^{(t)} \times \mathcal{Q}_h^{(t)}, \tag{3.3}$$

where $\mathcal{R}^{\text{VMS}}((\boldsymbol{\varphi}_h, q_h), (\boldsymbol{u}_h, p_h); \widehat{\boldsymbol{u}}_h)$ is defined as:

$$\begin{aligned}
\mathcal{R}^{\text{VMS}}((\boldsymbol{\varphi}_h, q_h), (\boldsymbol{u}_h, p_h); \widehat{\boldsymbol{u}}_h) := \mathcal{B}((\boldsymbol{\varphi}_h, q_h), (\boldsymbol{u}_h, p_h); \widehat{\boldsymbol{u}}_h) - \mathcal{F}(\boldsymbol{\varphi}_h, q_h) \\
+ \sum_{T \in \mathcal{T}_h} \Big[\, ((\boldsymbol{u}_h - \widehat{\boldsymbol{u}}_h) \cdot \nabla \boldsymbol{\varphi}_h, \tau_M Res_M(\boldsymbol{u}_h, p_h))_{\mathrm{L}^2(T)} \\
+ (\nabla \cdot \boldsymbol{\varphi}_h, \tau_C Res_C(\boldsymbol{s}_h))_{\mathrm{L}^2(T)} \\
+ \big((\boldsymbol{u}_h - \widehat{\boldsymbol{u}}_h) \cdot \nabla \boldsymbol{\varphi}_h^T, \tau_M Res_M(\boldsymbol{u}_h, p_h)\big)_{\mathrm{L}^2(T)} \\
- (\nabla \boldsymbol{\varphi}_h, \tau_M Res_M(\boldsymbol{u}_h, p_h) \otimes \tau_M Res_M(\boldsymbol{u}_h, p_h))_{\mathrm{L}^2(T)} \\
+ (\nabla q_h, \tau_M Res_M(\boldsymbol{u}_h, p_h))_{\mathrm{L}^2(T)} \Big] ,
\end{aligned} \tag{3.4}$$

with $\mathcal{B}((\boldsymbol{\varphi}_h, q_h), (\boldsymbol{u}_h, p_h); \widehat{\boldsymbol{u}}_h)$ defined in (2.6a) and $\mathcal{F}(\boldsymbol{\varphi}_h, q_h)$ in Eq. (2.6b); the residuals (in strong form) $Res_M(\boldsymbol{u}_h, p_h)$ and $Res_C(\boldsymbol{u}_h, p_h)$ and the parameters τ_M and τ_C are given by:

$$Res_M(\boldsymbol{u}_h, p_h) := \frac{\partial \boldsymbol{u}_h}{\partial t} + ((\boldsymbol{u}_h - \widehat{\boldsymbol{u}}_h) \cdot \nabla)\boldsymbol{u}_h + \nabla p_h - \frac{2}{\mathbb{R}e} \nabla \cdot (D(\boldsymbol{u}_h)) - \boldsymbol{f}, \tag{3.5a}$$

$$Res_C(\boldsymbol{u}_h, p_h) := \nabla \cdot \boldsymbol{u}_h, \tag{3.5b}$$

$$\tau_M := \left[\frac{4}{\Delta t^2} + (\boldsymbol{u}_h - \widehat{\boldsymbol{u}}_h) \cdot \boldsymbol{G} (\boldsymbol{u}_h - \widehat{\boldsymbol{u}}_h) + C_I \frac{1}{\mathbb{R}e^2} \boldsymbol{G} : \boldsymbol{G} \right]^{-\frac{1}{2}}, \tag{3.5c}$$

$$\tau_C := \frac{1}{\tau_M \boldsymbol{g} \cdot \boldsymbol{g}}, \tag{3.5d}$$

respectively, with $\boldsymbol{G}$ defined componentwise as $G_{i,j} := \sum_{k=1}^{d} \frac{\partial \eta_k}{\partial \mathrm{x}_i} \frac{\partial \eta_k}{\partial \mathrm{x}_j}$ for $i, j = 1, \ldots, d$, the covariant metric tensor related to the geometrical mapping with $\boldsymbol{\eta} = (\eta_1, \ldots, \eta_d)$, while $g_i := \sum_{k=1}^{d} \frac{\partial \eta_k}{\partial \mathrm{x}_i}$, for $i = 1, \ldots, d$. The constant $C_I > 0$ is independent of the mesh size, but depends on the degree p of the basis functions, and, following an element-wise inverse estimate, we set it as $C_I := 60 \cdot 2^{p-2}$ according to [66]; Δt refers to the time step size, even if we have not formally introduced the time discretization yet.

For the time discretization of the above problem (3.3), we use the generalized-α method [35, 66]. Specifically, the full discrete problem, which is implicit, is solved by a predictor-multicorrector algorithm at each time step; see e.g. [19].

4 Extended Nitsche's method (ENM) for mixed time varying (MTV) BCs

In this section, we introduce the ENM for the formulation of the Navier-Stokes equations with that account for valves functioning. Specifically, in Sec. 4.1, we focus on the aortic valve. In this respect, we introduce a proper set of BCs embedded in the weak formulation in the framework of the ENM. Such BCs are able both to describe the opening and closing of the aortic valve and to control the occurrence of the numerical instabilities due to the partial or total flow reversal associated to defective BCs of Sec. 2.4.2. Then, in Sec. 4.2, we propose a similar treatment for the BCs mimicking the mitral valve by using natural BCs [29] for the inflow; in this case, we add a suitable regularizing term to the BCs to model realistic inflow profiles.

4.1 MTV BCs: the extended Nitsche's method (ENM)

In order to introduce the ENM for the treatment of the aortic valve as MTV BCs of the Navier-Stokes equations in weak formulation, we follow the framework of [36] proposed for elliptic PDEs and then [61] for parabolic PDEs; for the original Nitsche's method, we refer the reader to [50]. We complement Eq. (2.1) with generalized Robin BCs on Γ^{AO} in the form:

$$-\boldsymbol{\Phi}(\boldsymbol{u} - \widehat{\boldsymbol{u}}; \boldsymbol{u}, p)\mathbf{n} + \gamma^{\mathrm{AO}}(\mathbf{x}, t)\boldsymbol{u}(\mathbf{x}, t) = \boldsymbol{G}(\mathbf{x}, t) + \gamma^{\mathrm{AO}}(\mathbf{x}, t)\boldsymbol{g}(\mathbf{x}, t) \quad \text{on } \Gamma^{\mathrm{AO}}, \tag{4.1}$$

where $\gamma^{\mathrm{AO}} : \Gamma^{\mathrm{AO}} \times (0, T) \to (0, +\infty)$, $\boldsymbol{G}$ is a function defining the defective BC described in Sec. 2.4.2 used for the open valve, and $\boldsymbol{g}$ defines the no-slip BC mimicking the closed valve (ideally, in a fixed ventricle, we have $\boldsymbol{g} = \mathbf{0}$). We notice that in the limit $\gamma \to 0$, Eq. (4.1) tends to the natural BC (2.3b), while, in the limit $\gamma \to \infty$, we recover the Dirichlet BC (2.3a). Finally, we recall that on $\Gamma^{\mathrm{W},(t)}$ for any $t \in (0, T)$ we impose the no-slip condition of Sec. 2.4 and on Γ^{MT} we prescribed a pulsatile periodic flow as described in Sec. 2.4.1, i.e. $\boldsymbol{u} = \boldsymbol{v}^{\mathrm{W}}$.

4.1.1 The ENM: application to the aortic valve

We consider the BC of Eq. (4.1) on Γ^{AO} in the semi-discrete spatial approximation of the Navier-Stokes equations (3.3) introduced in Sec. 3. Whereas, on $\partial\Omega^{(t)} \setminus \Gamma^{\mathrm{AO}} \equiv \Gamma^{\mathrm{W},(\mathrm{t})} \cup \Gamma^{\mathrm{MT}}$ we

strongly impose the essential BCs by defining the finite dimensional test and trial function spaces $\mathcal{V}_h^{(t)}$ and $\mathcal{W}_h^{(t)}$ as $\mathcal{V}_h^{(t)} := \mathcal{V}_{\overline{\boldsymbol{g}}}^{(t)} \cap \mathcal{N}_h^{(t)}$, $\mathcal{W}_h^{(t)} := \mathcal{W}^{(t)} \cap \mathcal{N}_h^{(t)}$, respectively, where, for $t \in (0,T)$:

$$\mathcal{V}_{\overline{\boldsymbol{g}}}^{(t)} := \{\boldsymbol{u} \in [\mathrm{H}^1(\Omega^{(t)})]^d : \boldsymbol{u} = \overline{\boldsymbol{g}} \quad \text{on } \Gamma^{\mathrm{W},(\mathrm{t})} \cup \Gamma^{\mathrm{MT}}\} \tag{4.2}$$

and

$$\mathcal{W}^{(t)} := \{\boldsymbol{u} \in [\mathrm{H}^1(\Omega^{(t)})]^d : \boldsymbol{u} = \boldsymbol{0} \quad \text{on } \Gamma^{\mathrm{W},(\mathrm{t})} \cup \Gamma^{\mathrm{MT}}\}, \tag{4.3}$$

with $\overline{\boldsymbol{g}} = \begin{cases} \boldsymbol{v}^{\mathrm{W}} & \text{on } \Gamma^{\mathrm{W},(\mathrm{t})}, \\ \boldsymbol{v}^{\mathrm{MT}} & \text{on } \Gamma^{\mathrm{MT}} \end{cases}$. In this manner, it is sufficient to look for a solution $\boldsymbol{u}$ of Eq. (3.3) in $[\mathrm{H}^1(\Omega^{(t)})]^d$ satisfying the BCs $\boldsymbol{u} = \overline{\boldsymbol{g}}$ on $\Gamma^{\mathrm{W},(\mathrm{t})} \cup \Gamma^{\mathrm{MT}}$ and for $t \in (0,T)$ by considering velocity test functions in $[\mathrm{H}^1(\Omega^{(t)})]^d$ vanishing on $\Gamma^{\mathrm{W},(\mathrm{t})} \cup \Gamma^{\mathrm{MT}}$.

Before introducing the weak imposition of the MTV BCs of Eq. (4.1) defined on Γ^{AO} by the ENM, we recall the notation introduced in Sec. 3.1. Let us consider the physical mesh $\mathcal{T}_h^{(t)}$ associated to the physical domain in the current configuration $\Omega^{(t)} \subset \mathbb{R}^d$; moreover, let the boundary $\Gamma^{(t)}$ be split into N_{eb} parts corresponding to the edges of the elements $T_b \subseteq \mathcal{T}_h^{(t)}$ such that $\partial T_b \cap \Gamma^{\mathrm{AO}} \neq \emptyset$, for $b = 1, \ldots, N_{eb}$. We define $\Gamma_b := \partial T_b \cap \Gamma^{\mathrm{AO}}$ and, for $d = 2$, we introduce the size h_b of Γ_b, for $b = 1, \ldots, N_{eb}$, by using the covariant element metric tensor $\mathbf{G}$ as:

$$h_b := 2(\boldsymbol{t}^T \mathbf{G} \boldsymbol{t})^{-1/2}, \tag{4.4}$$

where $\boldsymbol{t}$ is the unit vector tangent to the boundary element ∂T_b.

By considering a positive bounded time dependent real parameter $\xi > 0$, acting as a penalty parameter and associated to the stability properties of the method in case of flow reversal, the problem (3.3) with the weak imposition of the MTV BCs by means of the ENM reads:

find, for all $t \in (0,T)$, $\boldsymbol{u}_h(t) \in \mathcal{V}_h$ and $p_h(t) \in \mathcal{Q}_h$:

$$\mathcal{R}_h((\boldsymbol{\varphi}_h, q_h), (\boldsymbol{u}_h, p_h); \widehat{\boldsymbol{u}}) = \boldsymbol{0} \quad \forall (\boldsymbol{\varphi}_h, q_h) \in \mathcal{W}_h \times \mathcal{Q}_h, \tag{4.5}$$

where:

$$\begin{aligned}
\mathcal{R}_h((\boldsymbol{\varphi}, q), (\boldsymbol{u}, p), \widehat{\boldsymbol{u}}) := {} & \mathcal{R}^{\mathrm{VMS}}((\boldsymbol{\varphi}, q), (\boldsymbol{u}, p), \widehat{\boldsymbol{u}}) \\
& + \sum_{b=1}^{N_{eb}} \Bigg[\int_{\Gamma_b} \left(-\frac{\gamma h_b}{\xi + \gamma h_b} \right) \boldsymbol{\varphi} \cdot (\boldsymbol{\Phi}(\boldsymbol{u} - \widehat{\boldsymbol{u}}; \boldsymbol{u}, p)\mathbf{n}) \, \mathrm{d}\Gamma \\
& + \int_{\Gamma_b} \left(-\frac{\gamma h_b}{\xi + \gamma h_b} \right) (\boldsymbol{\Phi}^*_{in}(\boldsymbol{u} - \widehat{\boldsymbol{u}}; \boldsymbol{\varphi})\mathbf{n}) \cdot (\boldsymbol{u} - \boldsymbol{g}) \, \mathrm{d}\Gamma \\
& + \int_{\Gamma_b} \left(\frac{\xi\gamma}{\mathbb{R}e(\xi + \gamma h_b)} \right) \boldsymbol{\varphi} \cdot (\boldsymbol{u} - \boldsymbol{g}) \, \mathrm{d}\Gamma \\
& + \int_{\Gamma_b} \left(-\frac{\mathbb{R}e h_b}{\xi + \gamma h_b} \right) \boldsymbol{\Phi}^*_{in}(\boldsymbol{u} - \widehat{\boldsymbol{u}}; \boldsymbol{\varphi})\mathbf{n} \cdot (\boldsymbol{\Phi}(\boldsymbol{u} - \widehat{\boldsymbol{u}}; \boldsymbol{u}, p)\mathbf{n} - \boldsymbol{G}) \, \mathrm{d}\Gamma \\
& - \int_{\Gamma_b} \left(\frac{\xi}{\xi + \gamma h_b} \right) \boldsymbol{\varphi} \cdot \boldsymbol{G} \, \mathrm{d}\Gamma \Bigg],
\end{aligned} \tag{4.6}$$

with $\mathcal{R}^{\mathrm{VMS}}((\boldsymbol{\varphi}, q), (\boldsymbol{u}, p); \widehat{\boldsymbol{u}})$ defined in Eq. (3.4); $\boldsymbol{\Phi}^*_{in}$ is the *adjoint inflow total flux* , which, within the ALE formulation, reads $\boldsymbol{\Phi}^*_{in}(\boldsymbol{u} - \widehat{\boldsymbol{u}}; \boldsymbol{\varphi}) := (\boldsymbol{\varphi} \otimes (\boldsymbol{u} - \widehat{\boldsymbol{u}}))\chi_{\{(\boldsymbol{u} - \widehat{\boldsymbol{u}}) \cdot \mathbf{n} < 0\}} + \dfrac{2}{\mathbb{R}e} D(\boldsymbol{\varphi})$, for which $\boldsymbol{\Phi}^*_{in}(\boldsymbol{u} - \widehat{\boldsymbol{u}}; \boldsymbol{\varphi})\mathbf{n} = \{(\boldsymbol{u} - \widehat{\boldsymbol{u}}) \cdot \mathbf{n}\}_- \cdot \boldsymbol{\varphi} + \dfrac{2}{\mathbb{R}e} D(\boldsymbol{\varphi})\mathbf{n}$, where $\{(\boldsymbol{u} - \widehat{\boldsymbol{u}}) \cdot \mathbf{n}\}_- = \dfrac{(\boldsymbol{u} - \widehat{\boldsymbol{u}}) \cdot \mathbf{n} - |(\boldsymbol{u} - \widehat{\boldsymbol{u}}) \cdot \mathbf{n}|}{2}$.

The adjoint inflow total flux $\boldsymbol{\Phi}^*_{in}$ has been introduced in analogy with the weak enforcement of the Dirichlet BC for the advection-diffusion equation of [7] to handle the BCs for the inflow and outflow subsets of the boundary. In this manner, if Γ_b lays on an outflow boundary (for which $\boldsymbol{u}\cdot\mathbf{n}>0$), only the diffusive part of the total flux operator $\boldsymbol{\Phi}$ is considered for the weighting function $\boldsymbol{\varphi}$, while, if Γ_b is on an inflow boundary, we take into account both the diffusive and advective parts for the weighting function $\boldsymbol{\varphi}$.

We highlight that, by considering the ENM of Eq. (4.5) in the limit for $\gamma\to\infty$, we recover the original weak imposition of the Dirichlet BCs for the Navier-Stokes equations (2.1) presented in [7] in the ALE case. Contrarily, in the limit $\gamma\to 0$ in Eq. (4.5), we are weakly imposing natural BCs, even if we get an additional term with respect to the standard formulation; this latter term does not affect the consistency of the method, but rather assumes a stabilization role preventing the occurrence of the numerical instabilities caused by the partial or total flow reversal through Γ^{AO}. This term can be compared to the artificial traction term weakly added for the method proposed in [6] and further developed in [49] to prevent backflow divergence.

Remark 4.1. We observe that for $\gamma\to\infty$, i.e. for the weak imposition of the essential BCs on Γ^{AO}, the larger the value of ξ, the stronger the penalization associated to such BCs. Conversely, for $\gamma\to 0$, thus considering the imposition of the natural BCs on Γ^{AO}, the smaller the value of ξ, the larger the contribute of the stabilization term preventing backflow divergence. Therefore, similarly to γ, we also consider ξ as a time dependent real positive function $\xi:(0,T)\to\mathbb{R}:t\mapsto\xi(t)$. Specifically, we suppose ξ to be a measurable bounded function for which there exist two positive constants such that $0<\overline{\xi}_0<\xi(\mathbf{x},t)<+\infty$ and $0<\xi(\mathbf{x},t)<\overline{\xi}_\infty<+\infty$ for all $(\mathbf{x},t)\in\bigcup_{b=1}^{N_b^h}\Gamma_b\times(0,T)$. We observe that, the constant $\overline{\xi}_0$ can not assume arbitrary positive values, but, in order to ensure stability at the discrete level, it must be larger than some positive constant dependent on the data of the problem (i.e. the Reynolds number $\mathbb{R}e$ and the shape of the domain), on local boundary inverse estimates, and on the order of interpolation used in the finite dimensional space; see [7, 15].

4.2 MTV BCs for inflow boundaries: the mitral valve

Boundaries which are mainly associated with inflows can be treated in a manner which is analogous to the case described in Sec. 4.1. This is the case of the mitral valve, which for an idealized LV is treated as a MTV BC, similarly to Eq. (4.1). Indeed, when the mitral valve is open, one can set natural BCs (e.g. resistance BC), while, when it is closed, Dirichlet BCs. Using Dirichlet BCs for the full heart beat corresponds to assume for the mitral valve a given inflow velocity profile, which, as a matter of fact, should be an unknown of the problem. The use of the MTV BCs prevents the need to make such choice a priori, since a natural BC can be weakly set with an open valve. Nevertheless, such natural BC may still lead to unrealistic velocity profiles at the mitral valve because the standard resistance BC is too simple to account for the inflow, especially in a moving domain.

In order to prevent unrealistic inflow profiles, we add to the MTV BC of Eq. (4.1) a regularization term; this has the role of weakly penalizing the inflow velocity profiles which are too dissimilar from the parabolic one. Therefore, for the mitral valve, we propose on Γ^{MT} a generalized Robin BC with penalization based on the second-order Laplace-Beltrami operator, reading:

$$-\boldsymbol{\Phi}(\boldsymbol{u}-\widehat{\boldsymbol{u}};\boldsymbol{u},p)\mathbf{n}+\gamma^{\mathrm{MT}}(\mathbf{x},t)\boldsymbol{u}(\mathbf{x},t)-\alpha^{\mathrm{MT}}\triangle_\Gamma u=\boldsymbol{G}(\mathbf{x},t)+\gamma^{\mathrm{MT}}(\mathbf{x},t)\boldsymbol{g}(\mathbf{x},t)\quad\text{on }\Gamma^{\mathrm{MT}},\tag{4.7}$$

where α^{MT} is a positive real parameter constant in time.

At the discrete level, the BC (4.7) can be treated by means of the ENM as in Sec. 4.1.1, with the addition of the regularization term. Therefore, we consider for Eq. (3.3) the time dependent trial solution and weighting spaces for $t \in (0, T)$:

$$\mathcal{V}^{(t)} := \{\boldsymbol{u} \in (\mathrm{H}^1(\Omega^{(t)}) : \boldsymbol{u} = \boldsymbol{v}^{\mathrm{W}} \quad \text{on } \Gamma^{\mathrm{W},(\mathrm{t})}\} \tag{4.8}$$

and

$$\mathcal{W}^{(t)} := \{\boldsymbol{u} \in (\mathrm{H}^1(\Omega^{(t)}) : \boldsymbol{u} = \boldsymbol{0} \quad \text{on } \Gamma^{\mathrm{W},(\mathrm{t})}\}, \tag{4.9}$$

respectively. In this case, we account for $\Gamma^{\mathrm{V}} := \Gamma^{\mathrm{AO}} \cup \Gamma^{\mathrm{MT}}$ as a subset in which natural BCs are prescribed and we consider the N_{eb} elements such that $\partial T_b \cap \Gamma^{\mathrm{V}} \neq \emptyset$ for $b = 1, \dots, N_{eb}$. Then, the problem reads as in Eq. (4.5), where the residual of Eq. (4.6) is augmented by a regularizing term as:

$$\mathcal{R}'_h((\boldsymbol{\varphi}, q), (\boldsymbol{u}, p), \widehat{\boldsymbol{u}}) := \mathcal{R}_h((\boldsymbol{\varphi}, q), (\boldsymbol{u}, p), \widehat{\boldsymbol{u}}) + \sum_{b=1}^{N_{eb}} \left[-\alpha^{\mathrm{MT}} \int_{\Gamma_b} \chi_{\Gamma^{\mathrm{MT}}} \left(D(\boldsymbol{u}) : D(\boldsymbol{\varphi}) \right) \, \mathrm{d}\Gamma \right], \tag{4.10}$$

where $\chi_{\Gamma^{\mathrm{MT}}}(\mathbf{x}, t) := \begin{cases} 1 & \text{if } \mathbf{x} \in \Gamma^{\mathrm{MT}}, \\ 0 & \text{otherwise.} \end{cases}$

5 Numerical tests

We present the numerical study of the fluid dynamics in the idealized LV with prescribed wall motion. In Sec. 5.1 we assess the MTV BCs used to treat the aortic and mitral valve and we analyse the blood flow inside the LV. Then, we compare the flow patterns obtained with prescribed inflow profiles, parabolic or flat, at the mitral valve with those obtained with MTV BCs on both the valves, see Sec. 5.1.1. In Sec. 5.2, we study the role of the parameters involved in the MTV BCs and ENM. Specifically, we consider a prescribed parabolic pulsatile inlet profile at the mitral valve and the MTV BCs only for modelling the aortic valve. We perform a sensitivity analysis on the function γ^{AO} of Eq. (4.1) and compare the additional term preventing the numerical instabilities caused by flow reversal of Eq. (4.6) to the method proposed in [49] by showing the effectiveness of our formulation. Then, by using the MTV BCs to treat the mitral valve, we perform a sensitivity analysis on the parameter α^{MT} introduced in Eq. (4.10) and we show that the typical inlet jet profile is correctly identified.

We consider the time dependent domain $\Omega^{(t)}$ of Sec. 2.2, whose time dependent equatorial diameter $D(t)$ and height $H(t)$ are the solutions of the systems of ODEs (2.7). Specifically, by setting the initial configuration at the beginning of the diastolic phase, the initial conditions are set to $D(0) = D_0 = 3.4$ cm and $H(0) = H_0 = 2D_0$, yielding $D = 5.5$ cm and $H/D = 1.58$ at the end of the diastolic phase, the latter being the mean values of human LV healthy-normal subjects [2, 44]. The heart beat period is set as $T_{\mathrm{HB}} = 1.068$ s and the initial condition of the fluid velocity is set to the zero function, i.e. $\boldsymbol{u}(\mathbf{x}, 0) = \boldsymbol{u}_0 = \boldsymbol{0}$ in $\Omega^{(0)}$. Moreover, the blood is considered a Newtonian fluid with constant density $\rho = 1.06$ g/cm^3 and dynamic viscosity $\mu = 4 \cdot 10^{-2}$ g/(cm $\cdot$ s); the resistance constant is set to $C_{\mathrm{out}} = 0$. For our numerical study, we simulate up to ten heart beats and we disregard the initial three beats to remove non-physiological solutions from our analysis. The domain $\Omega^{(t)}$ is exactly represented by means of globally C^0-continuous NURBS basis functions of degree $p = 2$ with a mesh with $N_{\mathrm{el}} = 2{,}096$ elements, for a total of 9,576 Dofs for the velocity

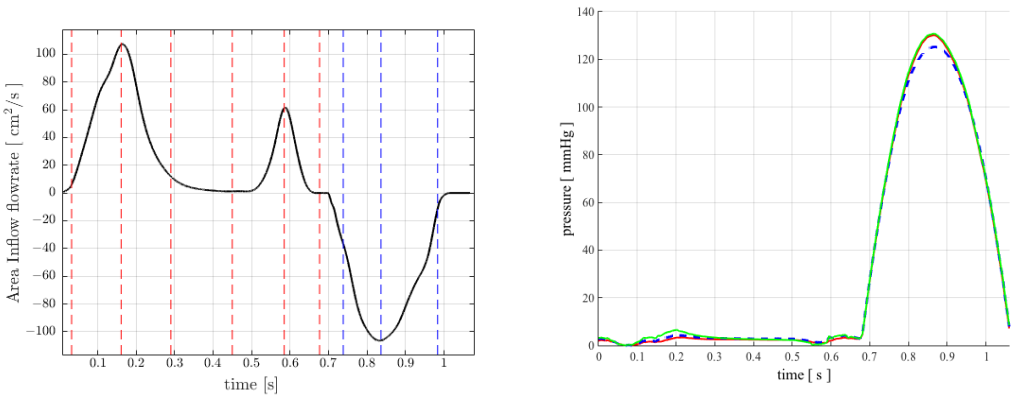

(a) (b)

Figure 3: (a) Times at which the numerical results are visualized during the heart beat for the diastolic (–) and systolic (–) phases. (b) Evolution of the pressure during the sixth heart beat in three points near the valves and LV base.

and pressure variables. Following [60], we define the time step by referring to the characteristic mesh size and velocity, corresponding to a dimensional time step equal to $\Delta t = 6.14 \cdot 10^{-3}$ s.

5.1 Blood flows in the LV

We describe the intraventricular blood flow pattern obtained by solving the Navier-Stokes equations endowed with the MTV BCs for the treatment of both the aortic and mitral valves. By referring to Eq. (4.10), we set $\xi^{\mathrm{AO}}(t) = 10^4 \chi_{[0,\ 0.68)}(t) + 10^2 \chi_{[0.68,\ 1.068)}(t)$, $\xi^{\mathrm{MT}}(t) = 10^2 \chi_{[0,\ 0.68)}(t) + 10^4 \chi_{[0.68,\ 1.068)}(t)$, $\gamma^{\mathrm{AO}}(t) = 10^{10} \chi_{[0,\ 0.68)}(t) + 10^{-7} \chi_{[0.68,\ 1.068)}(t)$, $\gamma^{\mathrm{MT}}(t) = 10^{-7} \chi_{[0,\ 0.68)}(t) + 10^{10} \chi_{[0.68,\ 1.068)}(t)$, and $\alpha^{\mathrm{MT}} = 100$. Ten cardiac cycles are simulated and we analyse both instantaneous quantities of interests as the velocity or pressure, for example at the sixth heart beat, and some phase averaged quantities over the last $N_{\mathrm{av}} = 7$ heart beats. The numerical results are shown at the characteristic times reported in Fig. 3a.

In Fig. 3b we report the evolution of the pressure field vs. the time in the sicth heart beat. The results are in agreement with the typical Wiggers diagram [48]. By using the same definitions of [13], we firstly consider the *phase average velocity* (reported in Fig. 4) which is defined as $\bar{\boldsymbol{u}}(\mathbf{x}, t) := \dfrac{1}{N_{\mathrm{av}}} \displaystyle\sum_{j=0}^{N_{\mathrm{av}}-1} \boldsymbol{u}(\mathbf{x}, t + jT_{\mathrm{HB}})$. In order to highlight the vortex structures we consider the Q-criterion which detects regions of positive values of the second invariant of the velocity gradient tensor where $Q = \dfrac{1}{2}\left(\|X\|_2^2 - \|S\|_2^2\right) > 0$, with $X = \dfrac{1}{2}\left(\nabla \boldsymbol{u} - \nabla \boldsymbol{u}^T\right)$ and $S = \dfrac{1}{2}\left(\nabla \boldsymbol{u} + \nabla \boldsymbol{u}^T\right)$; see e.g. [34, 59]. In Fig. 5 we report the results of the phase-averaged Q-criterion, say $\overline{Q}$-criterion. The transitional nature of the fluid from laminar to nearly turbulent over each heart beat and the cycle-to-cycle variations are quantitatively analysed by considering the *fluctuating kinetic energy* (E_{FKE}) (in Fig. 6) which is defined as $E_{\mathrm{FKE}} := \dfrac{1}{2} |\boldsymbol{u}_{\mathrm{rms}}(\mathbf{x}, t)|_2^2$, where $\boldsymbol{u}_{\mathrm{rms}}(\mathbf{x}, t) = \sqrt{\overline{\boldsymbol{u}^2}(\mathbf{x}, t) - \bar{\boldsymbol{u}}^2(\mathbf{x}, t)}$ is the *root mean square velocity* and $|\cdot|_2$ stands for the usual Euclidean norm.

The above results provide an insight of the blood flow patterns inside the LV. During the diastolic phase, the LV dilates and the cavity is filled with blood coming from the left atrium through the

mitral valve which is open. As showed in Fig. 3a, the mitral flow rate is characterized by a first peak (E-wave) corresponding to a rapid filling at $t = 0.16$ s and a second one (A-wave) in which the flow enters the chamber with a smaller velocity, due to the atrial contraction at $t = 0.58$ s; the two contro-rotating vortexes developing close to the mitral valve are clearly highlighted with the $\overline{Q}$-criterion. The strong jet entering the cavity forms a central vortex structure which dominates the entire flow field. Such vortex, which interacts with the jet entering through the mitral valve, induces a secondary one near the wall. This latter vortex is soon dissipated, while the primary vortex grows in intensity and dimensions moving toward the apex of the LV cavity. We notice also the presence of smaller vortices inside the LV cavity with an intense one at the apex. The phase averaged velocity $\overline{\boldsymbol{u}}$ also highlights the recirculations forming inside the LV. At the peak E-wave, as expected, a high velocity is observed in the proximity of the mitral valve. At the end of the diastolic phase the E_{FKE} reaches its largest values indicating large cycle-to-cycle variations and possible transitional behaviour of the flows from laminar to nearly turbulent. This results is in agreement with the numerical simulations and considerations of [13] for nearly realistic three-dimensional LV. At the systolic phase the aortic valve opens, while the mitral valve closes. The flow is naturally redirected towards the aortic valve and ejected from the LV. Moreover, a smaller region of recirculation under the mitral valve can be observed at the beginning of the ejection phase (Fig. 5). At this phase the vortexes are expelled from the LV and the flow regularized as highlighted both by the $\overline{Q}$-criterion and the E_{FKE} which presents smaller values.

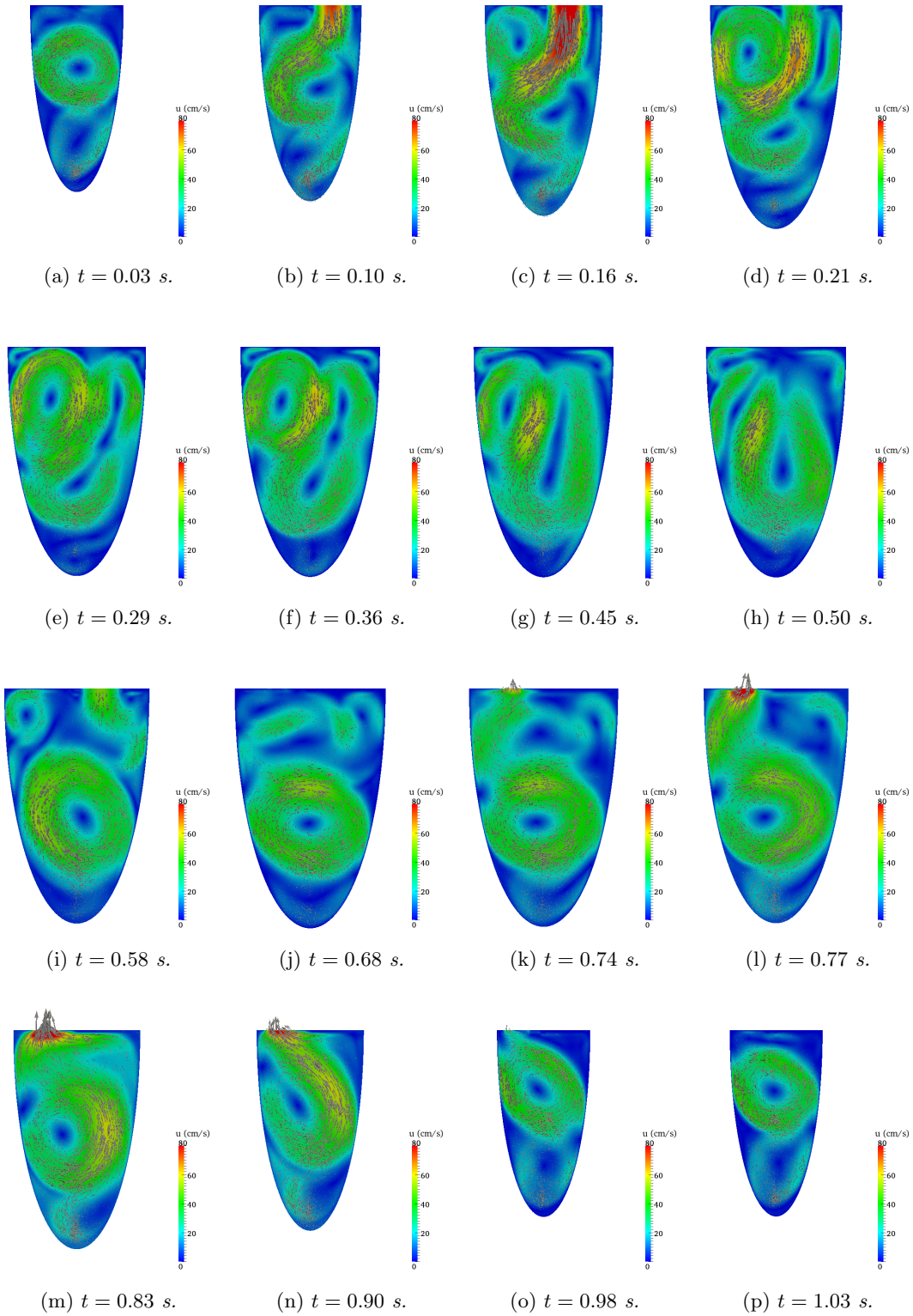

(a) $t = 0.03$ $s.$ (b) $t = 0.10$ $s.$ (c) $t = 0.16$ $s.$ (d) $t = 0.21$ $s.$

(e) $t = 0.29$ $s.$ (f) $t = 0.36$ $s.$ (g) $t = 0.45$ $s.$ (h) $t = 0.50$ $s.$

(i) $t = 0.58$ $s.$ (j) $t = 0.68$ $s.$ (k) $t = 0.74$ $s.$ (l) $t = 0.77$ $s.$

(m) $t = 0.83$ $s.$ (n) $t = 0.90$ $s.$ (o) $t = 0.98$ $s.$ (p) $t = 1.03$ $s.$

Figure 4: Phase averaged velocity magnitude $|\overline{\boldsymbol{u}}|$ (cm/s) at different instants of the heart beat (Fig. 3a).

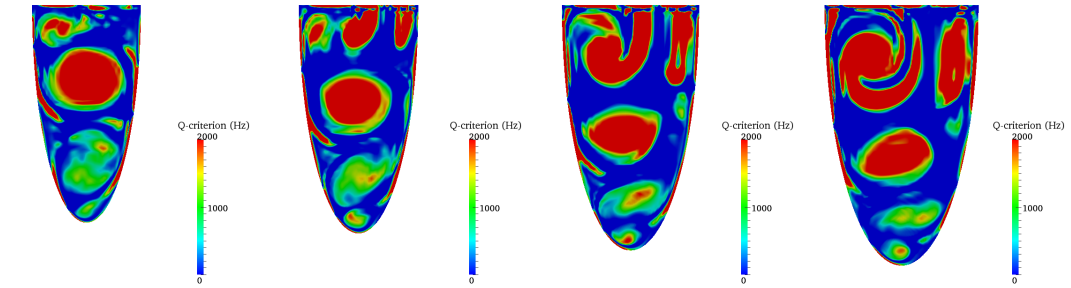

(a) $t = 0.03$ $s.$ (b) $t = 0.10$ $s.$ (c) $t = 0.16$ $s.$ (d) $t = 0.21$ $s.$

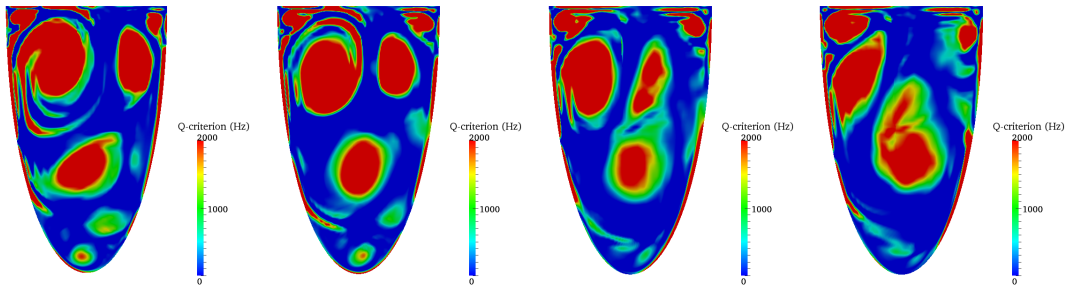

(e) $t = 0.29$ $s.$ (f) $t = 0.36$ $s.$ (g) $t = 0.45$ $s.$ (h) $t = 0.50$ $s.$

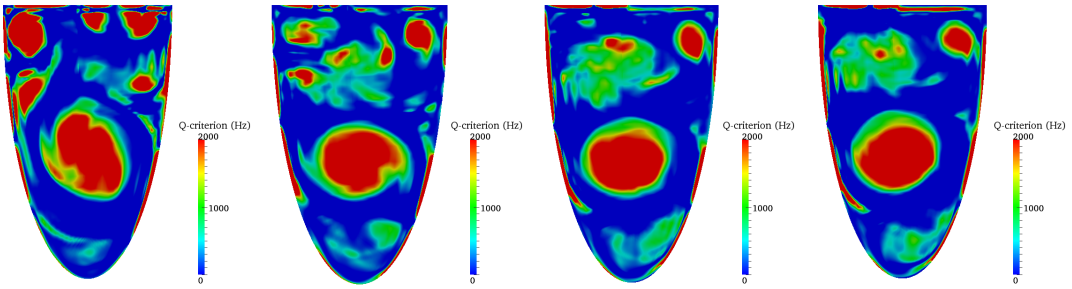

(i) $t = 0.58$ $s.$ (j) $t = 0.68$ $s.$ (k) $t = 0.74$ $s.$ (l) $t = 0.77$ $s.$

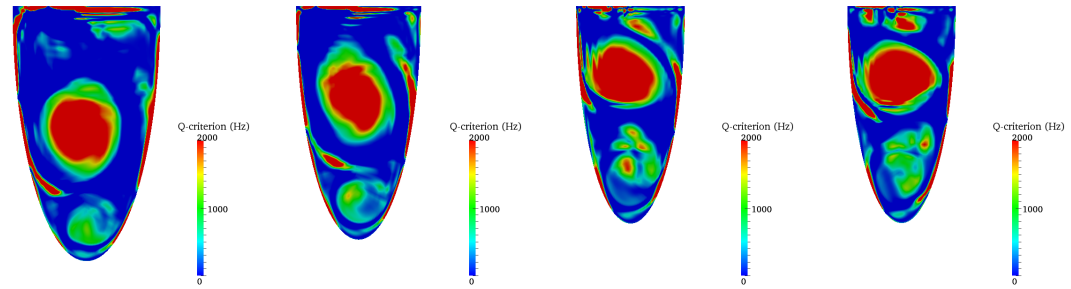

(m) $t = 0.83$ $s.$ (n) $t = 0.90$ $s.$ (o) $t = 0.98$ $s.$ (p) $t = 1.03$ $s.$

Figure 5: Phase averaged $\overline{Q}$-criterion (Hz) at different instants of the heart beat (Fig. 3a).

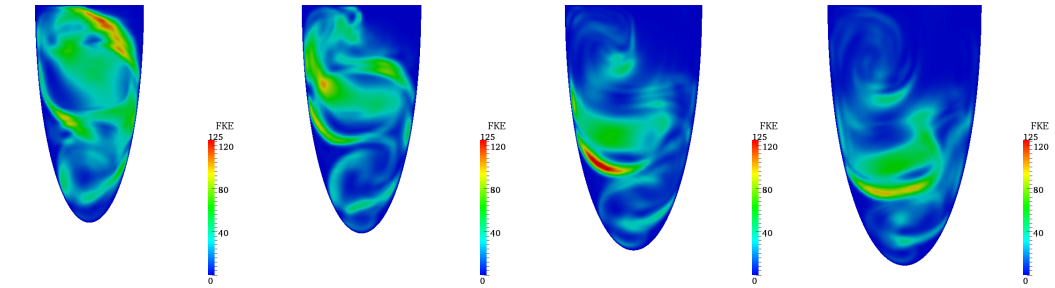

(a) $t = 0.03$ $s.$ (b) $t = 0.10$ $s.$ (c) $t = 0.16$ $s.$ (d) $t = 0.21$ $s.$

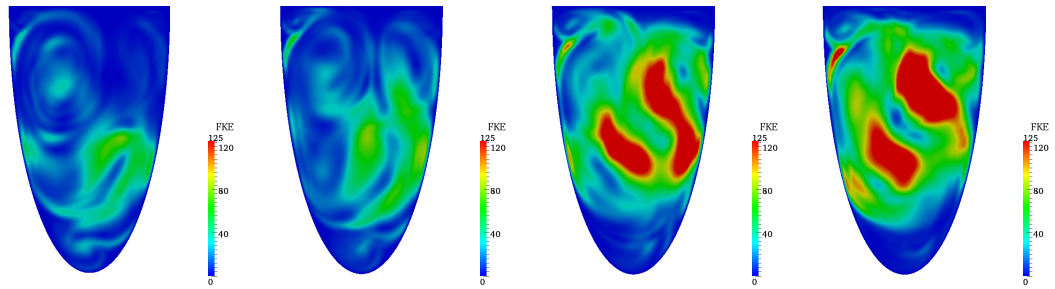

(e) $t = 0.29$ $s.$ (f) $t = 0.36$ $s.$ (g) $t = 0.45$ $s.$ (h) $t = 0.50$ $s.$

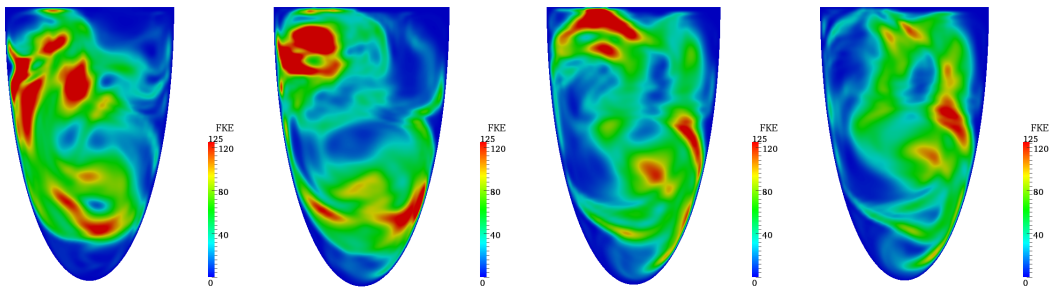

(i) $t = 0.58$ $s.$ (j) $t = 0.68$ $s.$ (k) $t = 0.74$ $s.$ (l) $t = 0.77$ $s.$

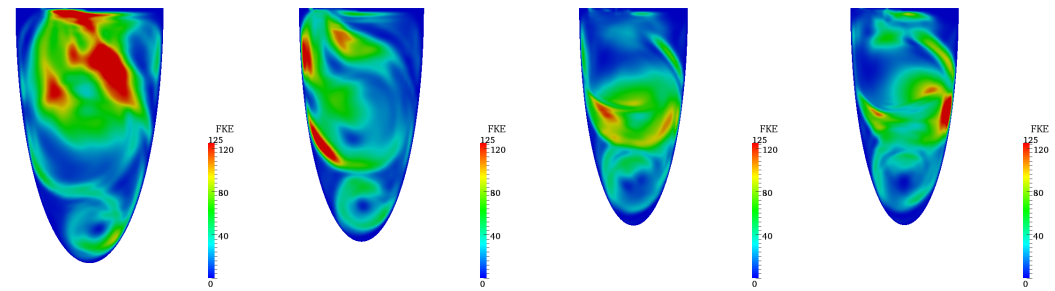

(m) $t = 0.83$ $s.$ (n) $t = 0.90$ $s.$ (o) $t = 0.98$ $s.$ (p) $t = 1.03$ $s.$

Figure 6: Fluctuating kinetic energy E_{FKE} (cm^2/s^2) at different instants of the heart beat (Fig. 3a).

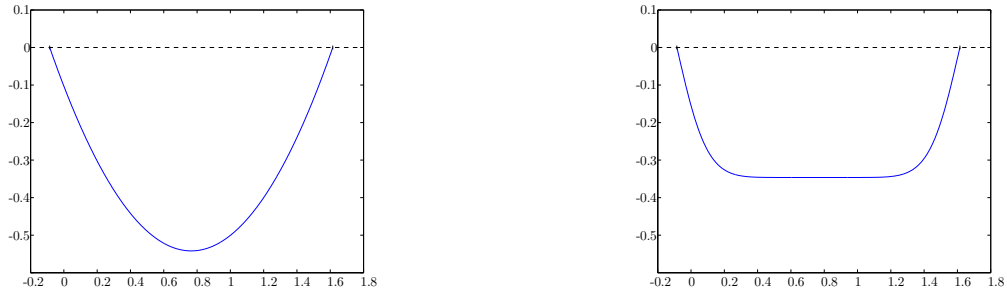

(a) Parabolic velocity profile.

(b) Flat velocity profile.

Figure 7: Imposed inflow velocity profiles through the mitral valve.

5.1.1 Comparison of results with different treatments of the BCs at the mitral valve.

We analyse the dependency of the intraventricular fluid dynamics on the inlet condition, especially for vortex structures as highlighted by flow visualizations [9, 55]. Specifically, we consider either the MTV BCs for modelling both the aortic and mitral valves or the strong imposition of inflow velocity at the mitral valve by considering either parabolic or flat profiles as shown in Fig. 7. In Figs. 8–10, we report the velocity magnitudes obtained in the three cases under consideration at the times reported in Fig. 3a and at the sixth heart beat. As expected, the velocity field and vortexes are significantly different during the diastolic phase, while more uniform at the systolic phase, i.e. when the flow is regularized during the ejection phase. Even if the inflow velocity profile of the MTV BCs is similar to the imposed parabolic one, the flow pattern are sensibly different, for which we highlight that the treatment of the mitral valve has a crucial importance in the study of the blood flows in the LV.

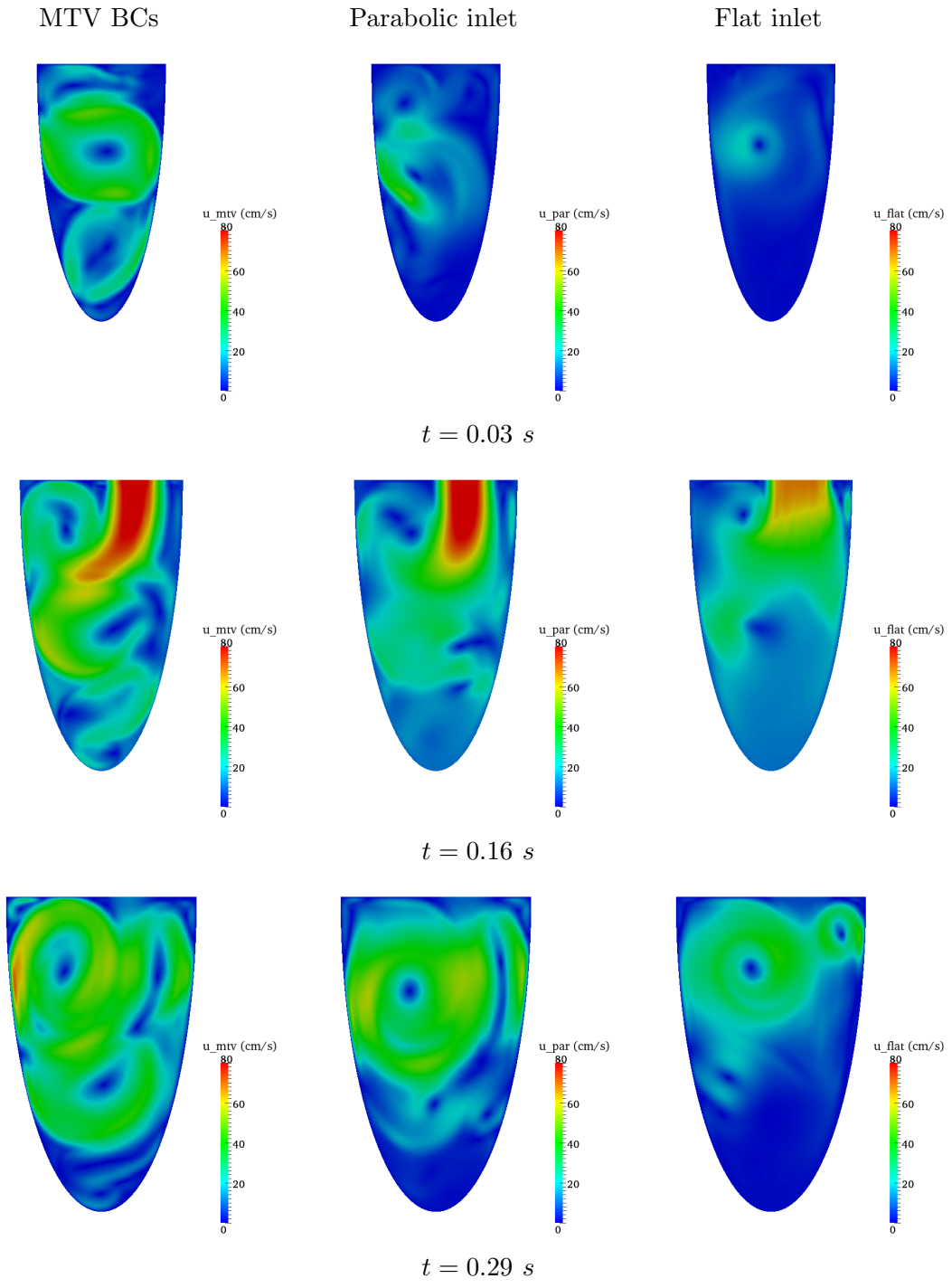

Figure 8: Magnitude of the velocity field $|\boldsymbol{u}|$ (cm/s) at different instants of the $\#6^{\text{-th}}$ heart beat for MTV BCs at the mitral valve (left), imposed parabolic (center), and flat (right) velocity profiles.

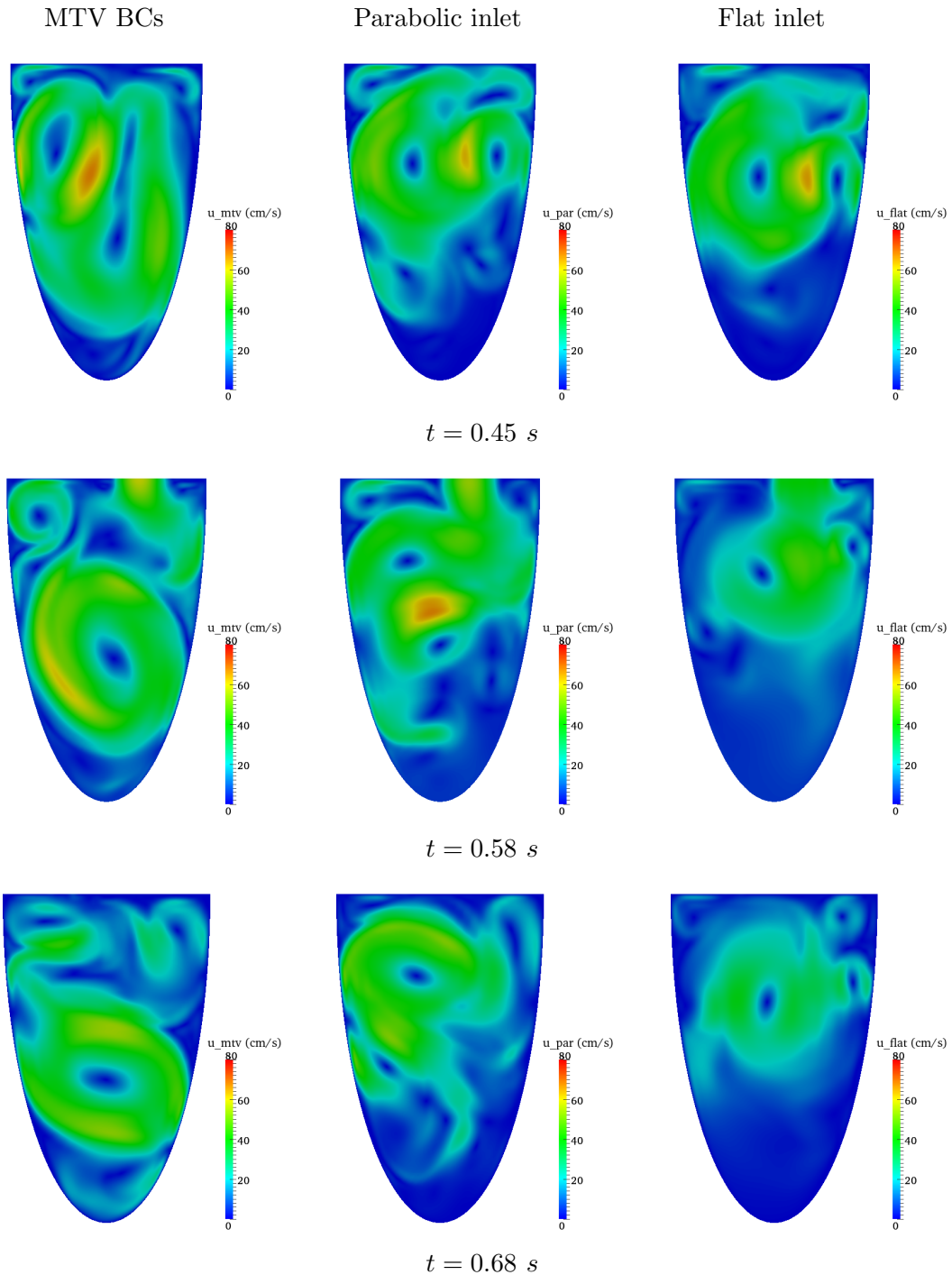

Figure 9: Magnitude of the velocity field $|\boldsymbol{u}|$ (cm/s) at different instants of the #6$^{\text{-th}}$ heart beat for MTV BCs at the mitral valve (left), imposed parabolic (center), and flat (right) velocity profiles.

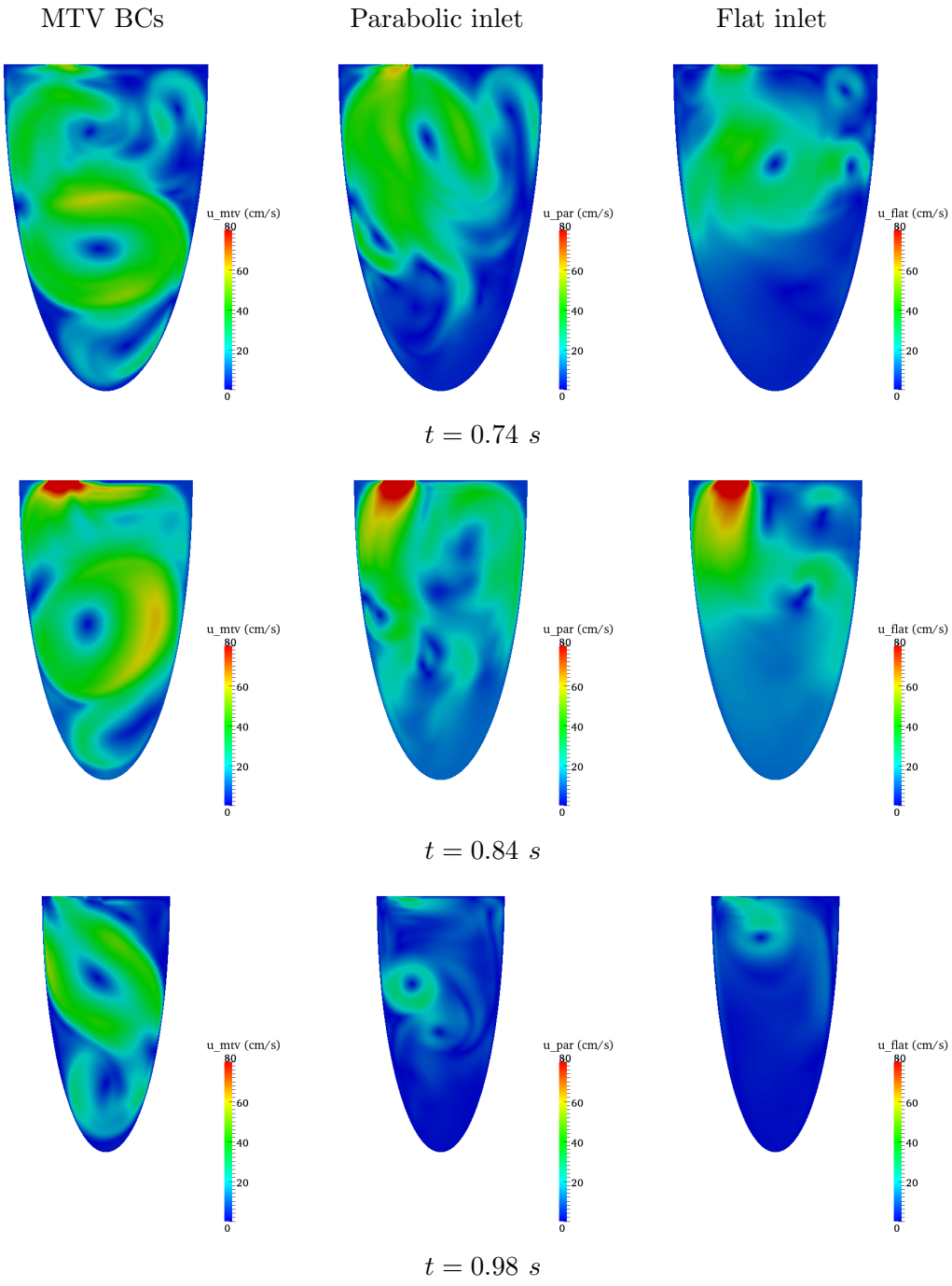

Figure 10: Magnitude of the velocity field $|\boldsymbol{u}|$ (cm/s) at different instants of the #6$^{\text{-th}}$ heart beat for MTV BCs at the mitral valve (left), imposed parabolic (center), and flat (right) velocity profiles.

5.2 Sensitivity to parameters

We analyse the dependency of our model on the time dependent function ξ^{AO} of Eq. (4.5), which both controls the penalization on the Dirichlet BC (for the closed valve) and manages the rule of the stabilizing term preventing numerical instabilities due to backflow divergence (for the open valve). We show that such terms effectively act as stabilizing terms preventing numerical instabilities due to backflow divergence and we compare the solution to the case of a "do-nothing" approach and to the method proposed by Bazilevs et al. in [6, 49]. In both the cases we consider the MTV BCs for modelling only the aortic valve and we impose an inflow parabolic profile at the mitral valve. Finally, we study the dependency on the parameter α^{MT} in Eq. (4.10) during the diastolic phase by considering MTV BCs for modelling the mitral valve.

5.2.1 Dependency on time dependent function ξ^{AO}

For the study of the function ξ^{AO} in the MTV BCs (4.5), we focus on the velocity profiles on the LV diameter corresponding to the aortic valve section. As observed in Remark 4.1, we consider a time dependent function to weakly enforce essential BCs or the resistance BC on Γ^{AO}.

As mentioned in Remark 4.1, we deduce that during the diastolic phase, for $\gamma^{\text{AO}} \to \infty$ (e.g. $\gamma^{\text{AO}} = 10^{10}$), the larger the value of ξ^{AO}, the larger is the penalization on the Dirichlet, and hence the better is the approximation of the Dirichlet data. The velocity profiles at the aortic valve reported in Fig. 11 numerically confirm the expected behaviour of the function ξ^{AO}, i.e. the larger is ξ^{AO}, the stronger is the enforcement of the Dirichlet BCs at the aortic valve during the diastolic phase. Nevertheless, we can notice in Fig. 12 that the amplitude of the oscillations caused by the choice of a small value of ξ^{AO} is negligible with respect to the values that the velocity takes at the time $t = 0.16$ s corresponding to the peak E-wave of the diastolic phase.

On the other hand, when considering the weak imposition of the resistance BCs for $\gamma \to 0$ (e.g. $\gamma^{\text{AO}} = 10^{-7}$) in Eq. (4.6), the smaller the value of ξ^{AO}, the larger is the contribute of the stabilizing term. This is highlighted in Fig. 13, where we observe that the velocity profiles are qualitatively similar for different values of γ^{AO} both during the early systole ($t = 0.74$ s) and at the peak systolic phase ($t = 0.84$ s), even if these may differ in the presence of backflow phenomena through Γ^{AO} at the late systolic phase. Specifically, the smaller the values of ξ^{AO}, the larger is the contribute of the term to prevent the insurgence of numerical instabilities associated to backflow divergence during the decelerating phase of the flow. We quantify the difference between solutions shown in Fig. 13d by computing the flowrate through the subsets of the boundary where $\boldsymbol{u} \cdot \mathbf{n} < 0$ which is equal to -3.76, -4.62, and -4.71 cm^2/s, respectively. We conclude that γ^{AO} should be "large"during the diastolic phase and "small"during the systolic phase.

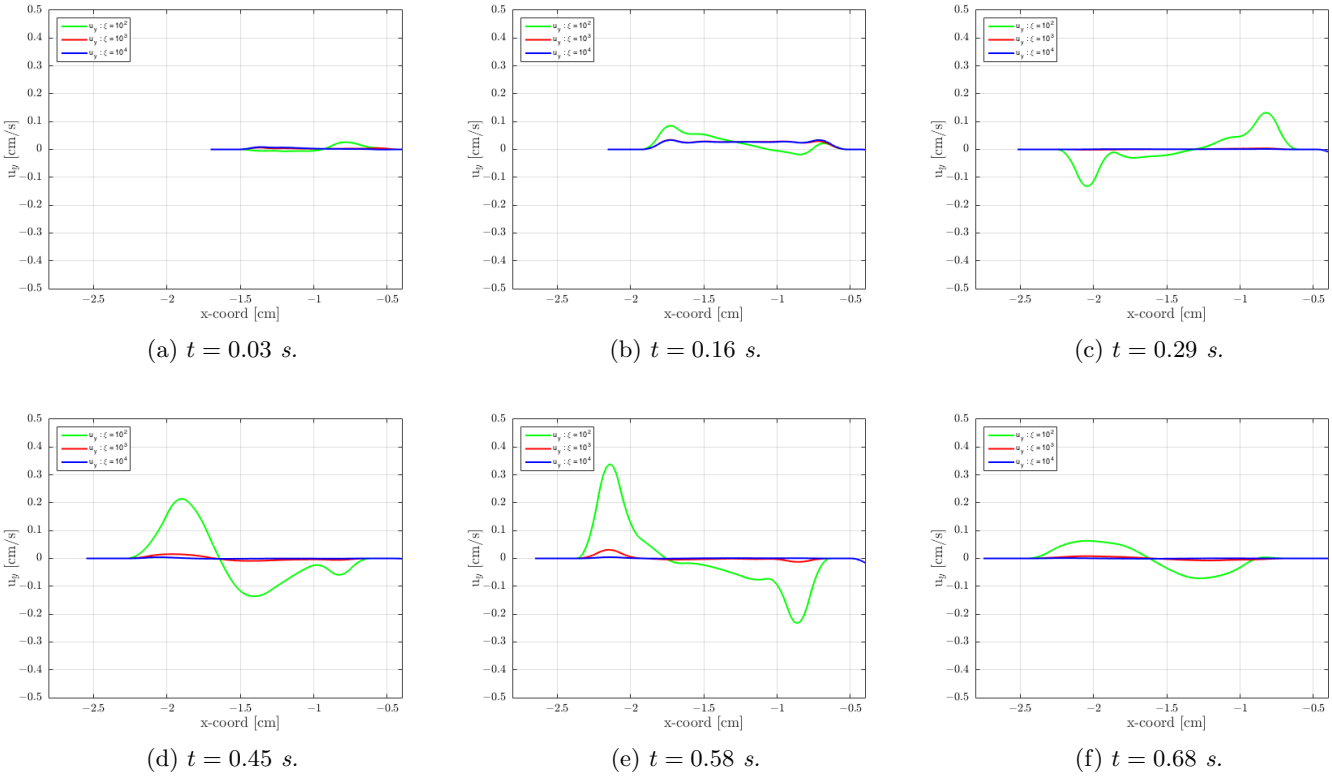

(a) $t = 0.03$ s. (b) $t = 0.16$ s. (c) $t = 0.29$ s.

(d) $t = 0.45$ s. (e) $t = 0.58$ s. (f) $t = 0.68$ s.

Figure 11: Outflow velocity profiles (at the LV base) during the diastolic phase at times $t \in [0, 0.68]$ s for different values of ξ^{AO}: $\xi^{\mathrm{AO}} = 10^2$ (–), $\xi^{\mathrm{AO}} = 10^3$ (–), and $\xi^{\mathrm{AO}} = 10^4$ (–) for $t \in [0, 0.68]$ s.

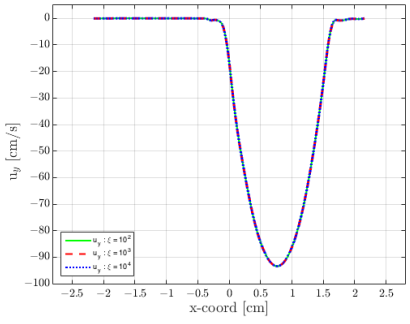

Figure 12: Inflow velocity profiles (at the LV base) for different values of ξ^{AO} at $t = 0.16$ s: $\xi^{\mathrm{AO}} = 10^2$ (–), $\xi^{\mathrm{AO}} = 10^3$ (–), and $\xi^{\mathrm{AO}} = 10^4$ (–).

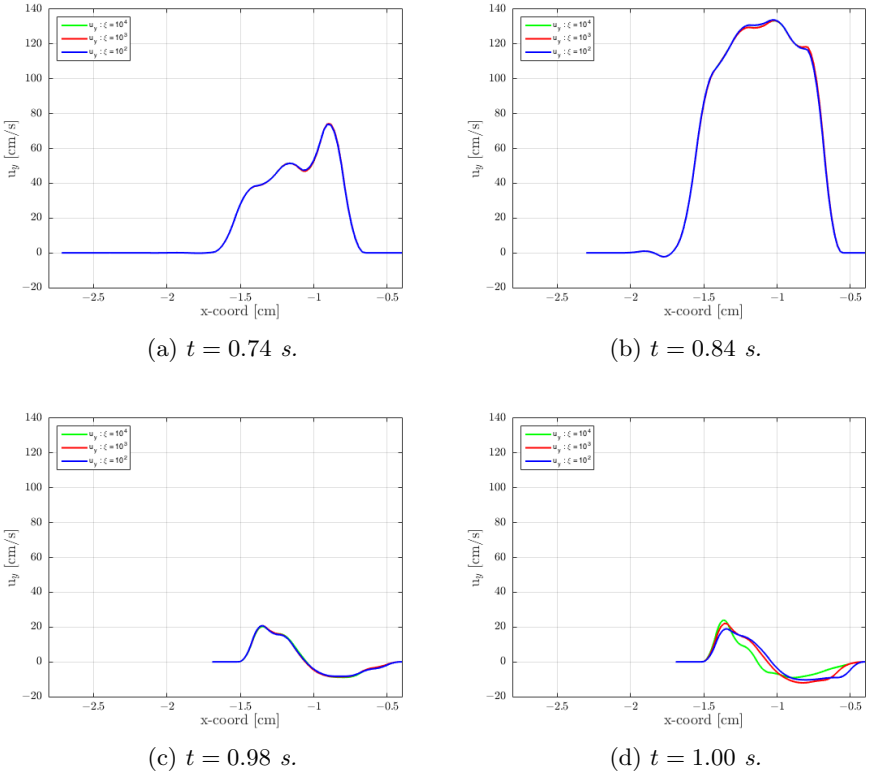

(a) $t = 0.74$ s. (b) $t = 0.84$ s.

(c) $t = 0.98$ s. (d) $t = 1.00$ s.

Figure 13: Outflow velocity profiles (at the LV base) during the systolic phase for different values of ξ^{AO} at times $t \in [0.68, 1.068)$ s: $\xi^{\text{AO}} = 10^4$ (–), $\xi^{\text{AO}} = 10^3$ (–), and $\xi^{\text{AO}} = 10^2$ (–).

5.2.2 Treatment of backflow at the aortic valve

We compare our formulation with the stabilization term for the outlet backflow with the method considered in [6, 49]. The latter is based on the introduction of an artificial outward traction term at the outlet boundary, i.e. acting in the direction opposite to backflow; this has been shown in [49] to be effective without altering significantly the local and global flow dynamics. Specifically, we compare the results obtained by our approach with those obtained with the method of [49]; for reference, we also report the results obtained without any treatment of backflows. In the comparison, we use the same discretization parameters and data to yield coherent results by focusing on the aortic valve.

In Figs. 14 and 15 we report the outflow velocity profiles at the LV base by comparing the results obtained by our method (ENM with MTV BCs) with those by the artificial traction of [49] and the standard resistance BCs (no treatment of backflows). We remark that our method better controls the backflows, even for the larger valve considered in Fig. 15, where we let the outflow track to grow larger accordingly with the dilatation map. We notice that, in the deceleration phase, the standard resistance BC shows an increasing reinflow on the part of the aortic valve near to the center of the cavity which causes the divergence of the numerical method after the time corresponding to $t = 0.90$ s (Fig. 15c). Contrarily, we can observe that the other two methods exhibit a qualitatively analogous profile and control the numerical instabilities due to backflow. We also stress the fact

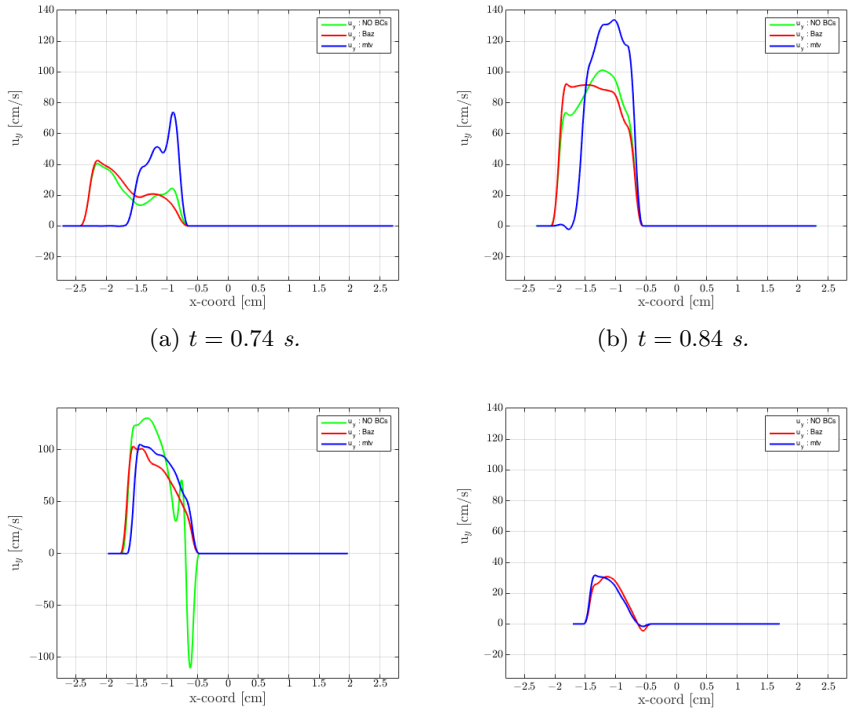

(a) $t = 0.74\ s.$ (b) $t = 0.84\ s.$

(c) $t = 0.90\ s.$ (d) $t = 0.98\ s.$

Figure 14: Outflow velocity profiles (u_{y}) through the aortic valve during the systolic phase; comparison of the results obtained with MTV BCs with backflow penalization (−), the artificial traction of [49] (−), and without any treatment of backflow (pure resistance BC) (−) at different time steps; we set $\xi^{\mathrm{AO}}(t) = 10^2$.

that our approach also allows to prevent flows through the outlet during the diastolic phase, i.e. when the aortic valve should be closed. Indeed, with the standard resistance condition and the artificial traction approach of [49] the net flux through the aortic valve at the diastolic phase is null, even if backflows are significant, as highlighted in Fig. 16; conversely, our method not only preserves the net flux (nearly null), but also ensure that $u_{\mathrm{y}} \simeq 0$ at Γ^{AO} at the diastolic phase.

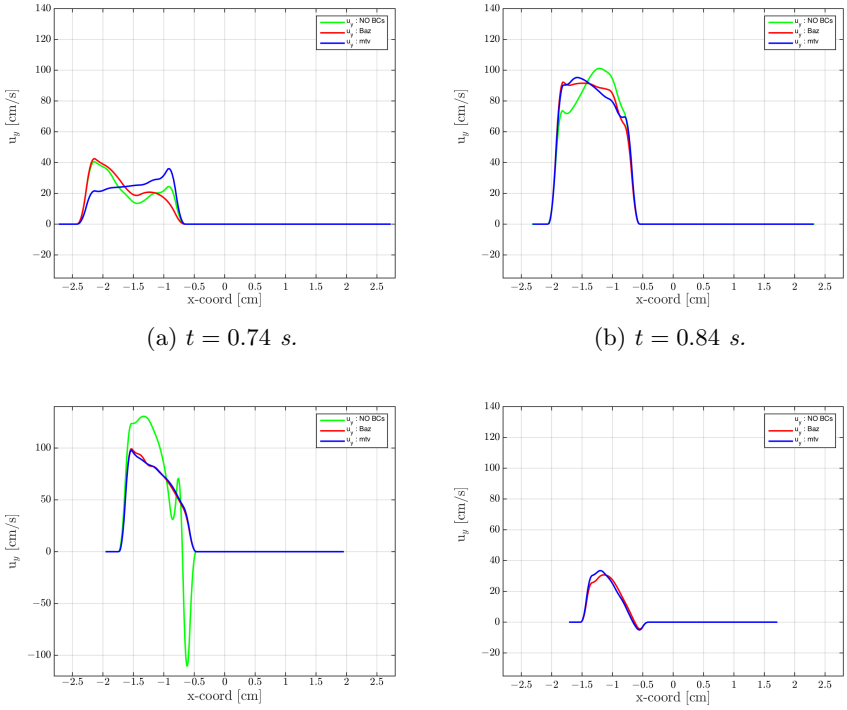

(a) $t = 0.74\ s.$ (b) $t = 0.84\ s.$

(c) $t = 0.90\ s.$ (d) $t = 0.98\ s.$

Figure 15: Outflow velocity profiles (u_y) through the aortic valve during the systolic phase; comparison of the results obtained with MTV BCs with backflow penalization (−), the artificial traction of [49] (−), and without any treatment of backflow (pure resistance BC) (−) at different instants; we set $\xi^{\mathrm{AO}}(t) = 10^2$.

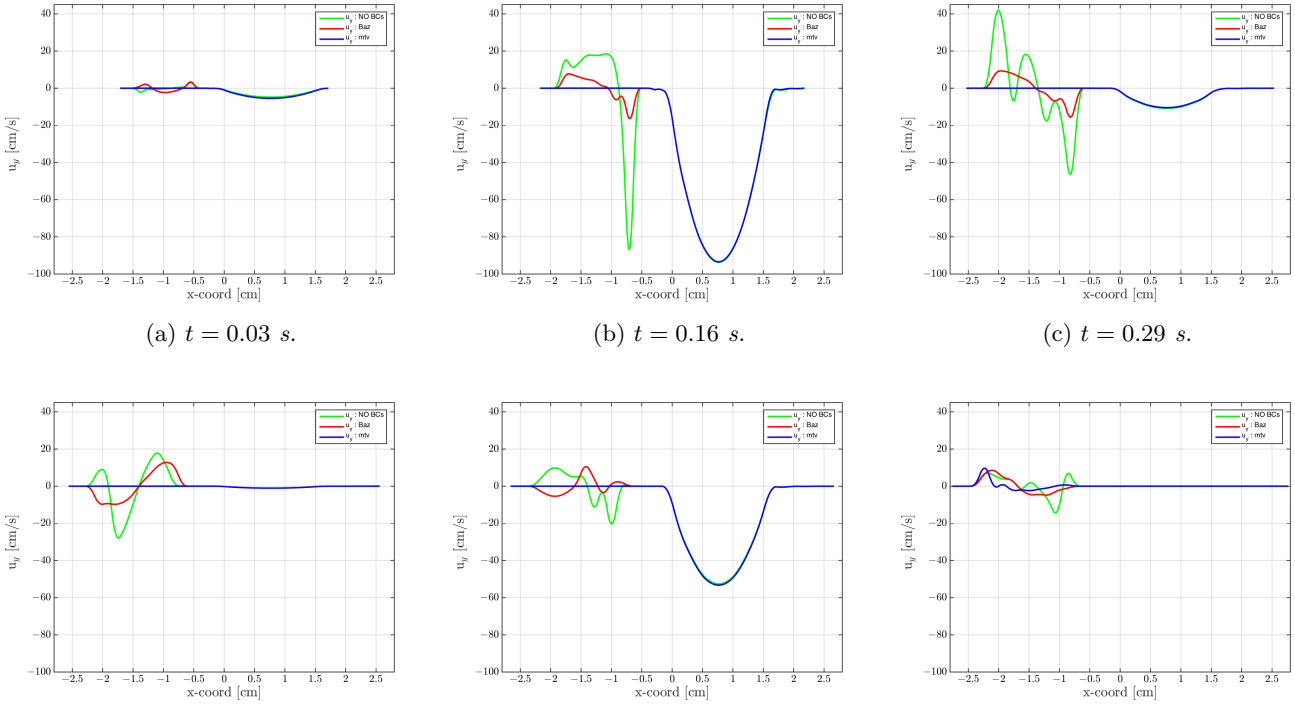

(a) $t = 0.03$ s. (b) $t = 0.16$ s. (c) $t = 0.29$ s.

(d) $t = 0.45$ s. (e) $t = 0.58$ s. (f) $t = 0.68$ s.

Figure 16: Velocity profiles (u_{y}) through the LV base the aortic valve during the diastolic phase; comparison of the results obtained with MTV BCs with backflow penalization (−), the artificial traction of [49] (−), and without any treatment of backflow (pure resistance BC) (−) at different instants; we set $\xi^{\mathrm{AO}}(t) = 10^4$.

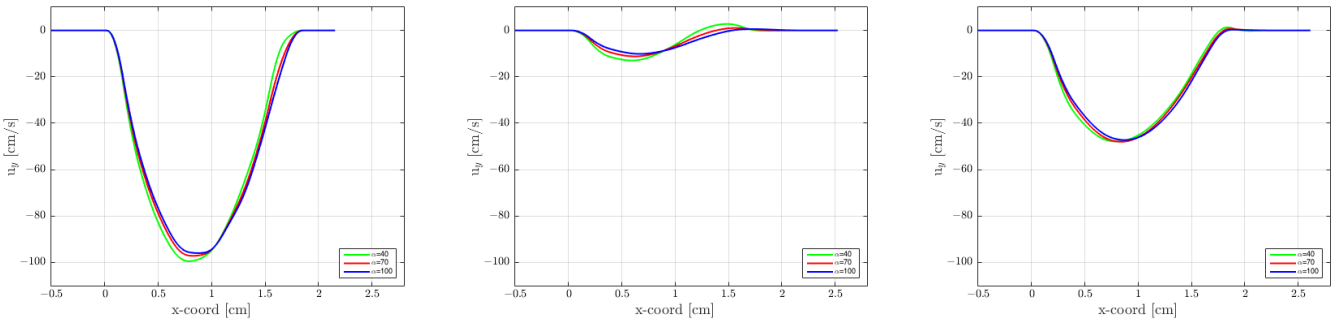

(a) $t = 0.16$ s. (b) $t = 0.29$ s. (c) $t = 0.58$ s.

Figure 17: Inflow velocity profiles at different times for different values of the α^{MT} parameter through the mitral valve; specifically, we set $\alpha^{\mathrm{MT}} = 40$ (−), $\alpha^{\mathrm{MT}} = 70$ (−), and $\alpha^{\mathrm{MT}} = 100$ (−).

5.2.3 Sensitivity analysis on α^{MT}

We analyse the role of the parameter α^{MT} in Eq. (4.10) during the diastolic phase. In Fig. 17 we notice that at the times corresponding to the peak E- and A-waves the inlet velocity profile is not significantly affected by the value of the parameter α, set equal to 40, 70 and 100, respectively. Moreover, we recover an inlet profile similar to the parabolic one of Fig. 7a, even if skewed similarly to [9, 55]. The maximum transmitral velocity achieved is correctly close to the realistic values [30]; specifically, we obtain $V_0 = -99.5$, -97.0, and -96.0 cm/s for for $\alpha^{\mathrm{MT}} = 40$, 70, and 100, respectively. Contrarily, there is some sensitivity of the formulation in the time interval comprised between $(0.16, 0.58)$. Specifically, in the decelerating phase of the first inlet jet, e.g. at $t = 0.29$ in Fig. 17b, we can observe that the higher the parameter α^{MT}, the more parabolic is the inlet shape profile and the less is the reoutflow, representing a reversal pathological condition with the flow which undergoes a re-injection into the atrial cavity.

6 Conclusions

We proposed MTV BCs for the treatment of the heart valves as BCs of the Navier-Stokes equations. Specifically, we introduced a weak formulation of such MTV BCs based on the ENM [36]. The proposed formulation allows an efficient and straightforward numerical treatment of time varying BCs which mimic the opening and closing phases of the valves, mathematically corresponding to different kind of BCs, namely natural and essential. Moreover, the additional consistency term stemming from the proposed method with respect to a standard weak formulation of natural BCs yields a stabilization term preventing the numerical instabilities associated to backflows at the outflow boundary. We numerically simulated the blood flows in idealized LV with prescribed wall movements and the MTV BCs. We critically discussed the results and compares them with those available in literature; a sensitivity analysis with respect to the parameters of the proposed method was also performed to highlight the efficiency and robustness of the method.

References

[1] B. Baccani, F. Domenichini, and G. Pedrizzetti. Vortex dynamics in a model left ventricle during filling. *European Journal of Mechanics – B/Fluids*, **21**:527–543, 2002.

[2] B. Baccani, F. Domenichini, G. Pedrizzetti, and G. Tonti. Fluid dynamics of the left ventricular filling in dilated cardiomyopathy. *Journal of Biomechanics*, **35**:665–671, 2002.

[3] Y. Bazilevs, L. Beirão da Veiga, J.A. Cottrell, T.J.R. Hughes, and G. Sangalli. Isogeometric Analysis: approximation, stability, and error estimates for h-refined meshes. *Mathematical Models and Methods in Applied Sciences*, **16**:1031–1090, 2006.

[4] Y. Bazilevs, V.M. Calo, J.A. Cottrell, T.J.R. Hughes, A. Reali, and G. Scovazzi. Variational multiscale residual-based turbulence modeling for large eddy simulation of incompressible flows. *Computer Methods in Applied Mechanics and Engineering*, **197**:173–201, 2007.

[5] Y. Bazilevs, V.M. Calo, T.J.R. Hughes, and Y. Zhang. Isogeometric fluid-structure interaction: theory, algorithms and computations. *Computational Mechanics*, **43**:3–37, 2008.

[6] Y. Bazilevs, J.R. Gohean, T.J.R. Hughes, R.D. Moser, and Y. Zhang. Patient-specific Isogeometric fluid-structure interaction analysis of thoracic aortic blood flow due to implantation of the Jarvik 2000 left ventricular assist device. *Computer Methods in Applied Mechanics and Engineering*, **198**:3534–3550, 2009.

[7] Y. Bazilevs and T.J.R. Hughes. Weak imposition of Dirichlet boundary conditions in fluid mechanics. *Computers & Fluids*, **36**:12–26, 2007.

[8] Y. Bazilevs, C. Michler, V.M. Calo, and T.J.R. Hughes. Weak Dirichlet boundary conditions for wall-bounded turbulent flows. *Computer Methods in Applied Mechanics and Engineering*, **196**:4853–4862, 2007.

[9] B.J. Bellhouse. Fluid mechanics of a model mitral valve and left ventricle. *Cardiovascular Research*, **6**:199–210, 1972.

[10] F. Brezzi and M. Fortin. *Mixed and Hybrid Finite Element Methods*. Springer–Verlag, New York, 1991.

[11] P. Bogacki and L.F. Shampine. A 3(2) pair of Runge-Kutta formulas. *Applied Mathematics Letters*, **2**:1–9, 1989.

[12] R. Calderer and A. Masud. A multiscale stabilized ALE formulation for incompressible flows with moving boundaries. *Computational Mechanics*, **46**:185–197, 2010.

[13] C. Chnafa, S. Mendez, and F. Nicoud. Image-based large-eddy simulation in a realistic left heart. *Computers & Fluids*, **94**:173–187, 2014.

[14] J. Chung and G.M. Hulbert. A time integration algorithm for structural dynamics with improved numerical dissipation: the generalized-α method. *Journal of Applied Mechanics*, **60**:371–375, 1993.

[15] P.G. Ciarlet. *The Finite Element Method for Elliptic Problems*. North–Holland, Amsterdam, 1978.

[16] J.A. Cottrell, T.J.R. Hughes, and Y. Bazilevs. Isogeometric Analysis: CAD, finite elements, NURBS, exact geometry and mesh refinement. *Computer Methods in Applied Mechanics and Engineering*, **194**:4135–4195, 2005.

[17] J.A. Cottrell, T.J.R. Hughes, and Y. Bazilevs. *Isogeometric Analysis: Toward Integration of CAD and FEA*. John Wiley & Sons, Chichester, UK, 2009.

[18] J.A. Cottrell, T.J.R. Hughes, and A. Reali. Studies of refinement and continuity in Isogeometric structural analysis. *Computer Methods in Applied Mechanics and Engineering*, **196**:4160–4183, 2007.

[19] L. Dedè, M.J. Borden, and T.J.R. Hughes. Isogeometric analysis for topology optimization with a phase field model. *Archives of Computational Methods in Engineering*, **19**:427–465, 2012.

[20] F. Domenichini and G. Pedrizzetti. Intraventricular vortex flow changes in the infarcted left ventricle: numerical results in an idealised 3D shape. *Computer Methods in Biomechanics and Biomedical Engineering*, **14**:95–101, 2011.

[21] F. Domenichini, G. Pedrizzetti, and B. Baccani. Three-dimensional filling flow into a model left ventricle, *Journal of Fluid Mechanics*, **539**:179–198, 2005.

[22] F. Domenichini, G. Querzoli, A. Cenedese, and G. Pedrizzetti. Combined experimental and numerical analysis of the flow structure into the left ventricle, *Journal of Biomechanics*, **40**:1988–1994, 2007.

[23] J. Donea. Arbitrary Lagrangian-Eulerian finite element methods. In T.J.R. Hughes and T. Belytschko (Eds.), *Computational Methods for Transient Analysis*, **198**:473–516, 1983.

[24] J. Donea, P. Fasoli-Stella, and S. Giuliani. Lagrangian and Eulerian finite element techniques for transient fluid-structure interaction problems. *Transactions of the 4th SMIRT Conference*, **B**, 1977.

[25] J. Donea, S. Giuliani, and J.P. Halleux. An arbitrary Lagrangian-Eulerian finite element method for transient dynamic fluid-structure interactions. *Computer Methods in Applied Mechanics and Engineering*, **33**:689–723, 1982.

[26] A. Falahatpisheh and A. Kheradvar. High-speed particle image velocimetry to assess cardiac fluid dynamics in vitro: From performance to validation. *European Journal of Mechanics - B/Fluids*, **35**:2–8, 2012.

[27] L. Formaggia and F. Nobile. A stability analysis for the arbitrary Lagrangian Eulerian formulation with finite elements. *East-West Journal of Numerical Mathematics*, **7**:105–131, 1999.

[28] L. Formaggia and F. Nobile. Stability analysis of second-order time accurate schemes for ALE-FEM. *Computer Methods in Applied Mechanics and Engineering*, **193**:4097–4116, 2004.

[29] V. Gravemeier, A. Comerford, L. Yoshihara, M. Ismail, and W. Wall. A novel formulation for Neumann inflow boundary conditions in Biomechanics. *International Journal for Numerical Methods in Biomedical Engineering*, **28**:560–573, 2012.

[30] B.O. Haugen, S. Berg, K.M. Brecke, S.O. Samstad, S.A. Slørdahl, T. Skjærpe, and H. Torp. Velocity profiles in mitral blood flow based on three-dimensional freehand colour flow imaging acquired at high frame rate. *European Journal of Echocardiography*, **1**:252–256, 2000.

[31] J.G. Heywood, R. Rannacher, and S. Turek. Artificial boundaries and flux and pressure conditions for the incompressible Navier-Stokes equations. *International Journal for numerical methods in fluids*, **22**:325–352, 1996.

[32] G.R. Hong, G. Pedrizzetti, G. Tonti, P. Li, Z. Wei, J.K. Kim, A. Baweja, S. Liu, N. Chung, H. Houle, J. Narula, and M.A. Vannan. Characterization and quantification of vortex flow in the human left ventricle by contrast echocardiography using vector particle image velocimetry. *JACC: Cardiovascular Imaging*, **1**:705–717, 2008.

[33] M.-C. Hsu, I. Akkerman, and Y. Bazilevs. Wind turbine aerodynamics using ALE–VMS: validation and the role of weakly enforced boundary conditions. *Computational Mechanics*, **50**:499–511, 2012.

[34] J.C.R. Hunt, A.A. Wray, and P. Moin. Eddies, stream, and convergence zones in turbulent flows. *Center for Turbulence Research Report*, **CTR-S88**:193–208, 1988.

[35] K.E. Jansen, C.H. Whiting, and G.M. Hulbert. A generalized-α method for integrating the filtered Navier-Stokes equations with a stabilized finite element method. *Computer Methods in Applied Mechanics and Engineering*, **190**:305–319, 2000.

[36] M. Juntunen and R. Stenberg. Nitsche's method for general boundary conditions. *Mathematics of Computation*, **78**:1353–1374, 2009.

[37] S.S. Khalafvand, E.Y.K. Ng, L. Zhong, and T.K. Hung. Fluid-dynamics modelling of the human left ventricle with dynamic mesh for normal and myocardial infarction: preliminary study. *Computers in Biology and Medicine*, **42**:863–870, 2012.

[38] P.J. Kilner, G.-Z. Yang, A.J. Wilkes, R.H. Mohiaddin, D.N. Firmin, and M.H. Yacoub. Asymmetric redirection of flow through the heart. *Nature*, **404**:759–761, 2000.

[39] H.J. Kim, C.A. Figueroa, T.J.R. Hughes, K.E. Jansen, and C.A. Taylor. Augmented lagrangian method for constraining the shape of velocity profiles at outlet boundaries for three-dimensional finite element simulations of blood flow. *Computer Methods in Applied Mechanics and Engineering*, **198**:3551–3566, 2009.

[40] H.B. Kim, J.R. Hertzberg, and R. Shandas. Development and validation of echo PIV. *Experiments in Fluids*, **36**:455–462, 2003.

[41] W.Y. Kim, P.G. Walker, E.M. Pedersen, J.K. Poulsen, S. Oyre, K. Houlind, and A.P. Yoganathan. Left ventricular blood flow patterns in normal subjects: a quantitative analysis by three-dimensional magnetic resonance velocity mapping. *Journal of the American College of Cardiology*, **26**:224–238, 1995.

[42] S.J. Kovács, D.M. Mcqueen, and C.S. Peskin. Modelling cardiac fluid dynamics and diastolic function. *Philosophical Transactions of the Royal Society A.*, **359**:1299–1314, 2001.

[43] S. Krittian, U. Janoske, H. Oertel, and T. Böhlke. Partitioned fluid-solid coupling for cardiovascular blood flow: left-ventricular fluid mechanics. *Annals of Biomedical Engineering*, **38**:1426–1441, 2010.

[44] R.M. Lang, M. Bierig, R.B. Devereux, F.A. Flachskampf, E. Foster, P.A. Pellikka, M.H. Picard, M.J. Roman, J. Seward, J. Shanewise, S. Solomon, K.T. Spencer, M. St.John Sutton, and W. Stewart. Recommendations for chamber quantification. *European Journal of Echocardiography*, **7**:79–108, 2006.

[45] J.D. Lemmon and A.P. Yoganathan. Computational model of left heart diastolic function with fluid-structure interaction. *Journal of Biomechanical Engineering*, **122**:297–303, 2000.

[46] J.O. Mangual, E. Kraigher-Krainer, A. De Luca, L. Toncelli, A. Shah, S. Solomon, G. Galanti, F. Domenichini, and G. Pedrizzetti. Comparative numerical study on left ventricular fluid dynamics after dilated cardiomyopathy. *Journal of Biomechanics*, **46**:1611–1617, 2013.

[47] D.M. Mcqueen and C.S. Peskin. *Heart Simulation by an Immersed Boundary Method with Formal Second-order Accuracy and Reduced Numerical Viscosity.* in *Mechanics for a New Millennium*, Springer, Netherlands, 429–444, 2002.

[48] J.R. Mitchell and J.-Jr Wang. Expanding application of the Wiggers diagram to teach cardiovascular physiology. *Advances in Physiology Education*, **38**:170–175, 2014.

[49] M.E. Moghadam, Y. Bazilevs, T.-Y. Hsia, I.E. Vignon-Clementel, and A.L. Marsden. A comparison of outlet boundary treatments for prevention of backflow divergence with relevance to blood flow simulations. *Computational Mechanics*, **48**:277–291, 2011.

[50] J. Nitsche. Über ein Variationsprinzip zur Lösung von Dirichlet-Problemen bei Verwendung von Teilräumen, die keinen Randbedingungen unterworfen sind. *Abhandlungen aus dem Mathematischen Seminar der Universität Hamburg*, **36**:9–15, 1971.

[51] C.S. Peskin. Flow patterns around heart valves: a numerical method. *Journal of Computational Physics*, **10**:252–271, 1972.

[52] C.S. Peskin. Numerical analysis of blood flow in the heart. *Journal of Computational Physics*, **25**:220–252, 1977.

[53] C.S. Peskin and D.M. McQueen. A three-dimensional computational model of blood flow in the heart: I. Immersed elastic fibers in a viscous incompressible fluid. *Journal of Computational Physics*, **81**:372–405, 1989.

[54] A. Quarteroni. *Numerical Models for Differential Problems*. Springer–Verlag, Milan, 2014.

[55] H. Reul, N. Talukder, and W. Muller. Fluid mechanics of the natural mitral valve. *Journal of Biomechanics*, **14**:361–372, 1981.

[56] P. Reymond, F. Merenda, F. Perren, D. Rufenacht, and N. Stergiopulos. Validation of a one-dimensional model of the systemic arterial tree. *American Journal of Physiological Heart Circulation Physiology*, **297**:H208–H222, 2009.

[57] G. Savaré. Parabolic problems with mixed variable lateral conditions: an abstract approach. *Journal of Pure and Applied Mathematics*, **76**:321–351, 1997.

[58] P.P. Sengupta, G. Pedrizzetti, P.J. Kilner, A. Kheradvar, T. Ebbers, G. Tonti, A.G. Fraser, and J. Narula. Emerging Trends in CV Flow Visualization. *JACC: Cardiovascular Imaging*, **5**:305–316, 2012.

[59] B.K. Shivamoggi and G.J.F. van Heijst. The Okubo-Weiss criteria in two-Dimensional Hydrodynamic and Magnetohydrodynamic flows. *arXiv:1110.6190*, 2015 .

[60] A. Tagliabue. Isogeometric Analysis for reduced fluid–structure interaction models in Haemodynamic applications. Master Degree Thesis, Università degli Studi dell'Insubria, Italy, 2012. `http://infoscience.epfl.ch/record/183031/files/thesis_tagliabue_2012.pdf`.

[61] A. Tagliabue, L. Dedè, and A. Quarteroni. Nitsche's method for parabolic partial differential equations with mixed time varying boundary conditions. *ESAIM: Mathematical Modelling and Numerical Analysis*, (to appear), 2015. `http://dx.doi.org/10.1051/m2an/2015054`.

[62] K. Takizawa, Y. Bazilevs, and T.E. Tezduyar. Space-time and ALE-VMS techniques for patient-specific cardiovascular fluid-structure interaction modeling. *Archives of Computational Methods in Engineering*, **19**:171–225, 2012.

[63] C. Vergara. Nitsche's method for defective boundary value problems in incompressible fluid-dynamics. *Journal of Scientific Computing*, **46**:100–123, 2011.

[64] J.A. Vierendeels, K. Riemslagh, E. Dick, and P.R. Verdonck Computer simulation of intraventricular flow and pressure during diastole. *Journal of Biomechanical Engineering*, **122**:667–674, 2000.

[65] H. Watanabe, S. Sugiura, H. Kafuku, and T. Hisada. Multiphysics simulation of left ventricular filling dynamics using fluid-structure interaction finite element method. *Biophysical Journal*, **87**:2074–2085, 2004.

[66] C.H. Whiting. *Stabilized Finite Element methods for fluid dynamics using a hierarchical basis.* Master's thesis, Rensselaer Polytechnic Institute Troy, New York, 1999.

[67] X. Zheng, J.H. Seo, V. Vedula, T. Abraham, R. Mittal. Computational modeling and analysis of intracardiac flows in simple models of the left ventricle. *European Journal of Mechanics B/Fluids*, **35**:31–39, 2012.

Recent publications:

MATHEMATICS INSTITUTE OF COMPUTATIONAL SCIENCE AND ENGINEERING
Section of Mathematics
Ecole Polytechnique Fédérale
CH-1015 Lausanne

18.2015 DANIEL KRESSNER, MICHAEL STEINLECHNER, BART VANDEREYCKEN:
Preconditioned low-rank Riemannian optimization for linear systems with tensor product structure

19.2015 ALESSANDRO S. PATELLI, LUCA DEDÈ, TONI LASSILA, ANDREA BARTEZZAGHI, ALFIO QUARTERONI:
Isogeometric approximation of cardiac electrophysiology models on surfaces: an accuracy study with application to the human left atrium

20.2015 MATTHIEU WILHELM, LUCA DEDÈ, LAURA M. SANGALLI, PIERRE WILHELM:
IGS: an IsoGeometric approach for Smoothing on surfaces

21.2015 SIMONE DEPARIS, DAVIDE FORTI, PAOLA GERVASIO, ALFIO QUARTERONI:
INTERNODES: an accurate interpolation-based method for coupling the Galerkin solutions of PDEs on subdomains featuring non-conforming interfaces

22.2015 ABDUL-LATEEF HAJI-ALI, FABIO NOBILE, LORENZO TAMELLINI, RAÙL TEMPONE:
Multi-index stochastic collocation for random PDEs

23.2015 SIMONE BRUGIAPAGLIA, FABIO NOBILE, STEFANO MICHELETTI, SIMONA PEROTTO:
A theoretical study of COmpRessed SolvING for advection-diffusion-reaction problems

24.2015 ANA ŠUŠNJARA, NATHANAËL PERRAUDIN, DANIEL KRESSNER, PIERRE VANDERGHEYNST:
Accelerate filtering on graphs using Lanczos mehtod

25.2015 FRANCESCO BALLARIN, ELENA FAGGIANO, SONIA IPPOLITO, ANDREA MANZONI, ALFIO QUARTERONI, GIANLUIGI ROZZA, ROBERTO SCROFANI:
Fast simulation of patient-specific haemodynamics of coronary artery bypass grafts based on a Pod-Galerkin method and a vascular shape parametrization

26.2015 FRANCISCO MACEDO:
Benchmark problems on stochastic automata networks in tensor train format

27.2015 JONAS BALLANI, DANIEL KRESSNER:
Reduced basis methods: from low-rank matrices to low-rank tensors

28.2015 ALBERT COHEN, GIOVANNI MIGLIORATI, FABIO NOBILE:
Discrete least-squares approximations over optimized downward closed polynomial spaces in arbitrary dimension

29.2015 ABDUL-LATEEF HAJI-ALI, FABIO NOBILE, LORENZO TAMELLINI, RAÚL TEMPONE:
Multi-index stochastic collocation convergence rates for random PDEs with parametric regularity

30.2015 LAURA IAPICHINO, ALFIO QUARTERONI, GIANLUIGI ROZZA:
Reduced basis method and domain decomposition for elliptic problems in networks and complex parametrized geometries

31.2015 ANNA TAGLIABUE, LUCA DEDÈ, ALFIO QUARTERONI:
Fluid dynamics of an idealized left ventricle: the extended Nitsche's method for the treatment of heart valves as mixed time varying boundary conditions